SMHI PROMIS-RAPPORTER
Nr 11, Oktober 1990
PROMIS REPORTS

SMHI RMK
Nr 61, Oktober 1990

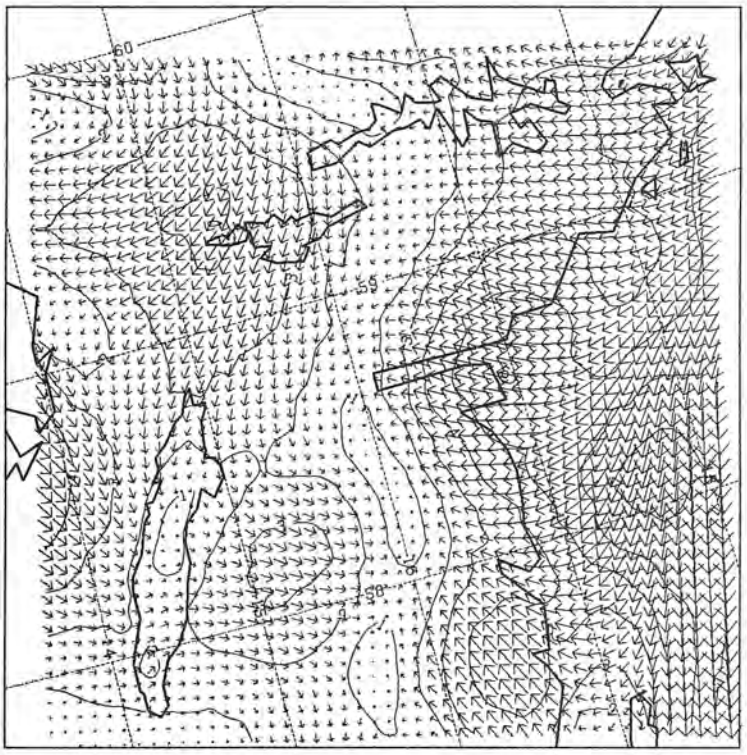

Meso-γ Scale Objective Analysis of Near Surface Temperature, Humidity and Wind and its Application in Air Pollution Modelling.

Lars Meuller, Lennart Robertson, Erik Andersson and Nils Gustafsson

SMHI PROMIS REPORTS Nr 11, Oktober 1990

SMHI REPORTS Nr 61, Oktober 1990

METEOROLOGY AND CLIMATOLOGY

Meso-γ Scale Objective Analysis of Near Surface Temperature, Humidity and Wind and its Application in Air Pollution Modelling.

Lars Meuller, Lennart Robertson, Erik Andersson and Nils Gustafsson

Printed in Sweden, SMHI Norrköping 1991

Issuing Agency
SMHI
S-601 76 Norrköping
SWEDEN

Report number
RMK 61

Report date
January 1991

Author (s)
Lars Meuller, SMHI
Lennart Robertsson, SMHI
Erik Andersson, ECMWF
Nils Gustafsson, SMHI

Title (and Subtitle)

Meso-γ Scale Objective Analysis of Near Surface Temperature, Humidity and Wind and its Application in Air Pollution Modelling

Abstract
Within the PROMIS project at the Swedish Meteorological and Hydrological Institute a meso-scale network of automatic weather observing stations was established for several purposes. For several of these applications it was considered advantageous to process the data by applying an objective analysis, including quality control, on the observed data to a regular grid.

The analysis system, which is in operational use since a couple of years, is described in this report. The system is based on the meso scale analysis system described in PROMIS Report Nr 1, modified to the finer resolution on the meso-γ scale.

In the analysis of the surface wind a new approach is used, where the wind is divided into a divergent and a non-divergent part, which is shown to give a better description of the local wind field.

The report also gives example of how the analysed fields can be used in dispersion modelling.

Key words
Optimum interpolation
Analysis
Meso scale

Supplementary notes

Number of pages
51

Language
English

ISSN and title
0347-2116 SMHI Reports Meteorology and Climatology

Report available from:
Swedish Meteorological and Hydrological Institute

CONTENTS

APPENDIX

1 Introduction

An objective analysis scheme for the meso-γ scale is described in this paper. The main objective of this scheme is to produce analysis fields of low level parameters, in the first instance 10 meter winds, for nowcasting and very short range forecasting purposes. The primary source of observational data for the analysis is a mesoscale network of automatic weather observing stations. The described meso-γ analysis scheme is one component of an experimental system for nowcasting and very short range forecasting, PROMIS 600, established within the central forecasting office of the Swedish Meteorological and Hydrological Institute. An overview of the analysis and forecasting tools for PROMIS 600 has been presented by Gustafsson and Törnevik [16]. The analysis scheme described in this paper is closely linked to the PROMIS 600 meso-β analysis scheme, described by Andersson et al [1].

The basic technique utilized for the meso-γ analysis is optimum interpolation, see Gandin [14]. Observed deviations from analysis first guess fields, provided by e.g. a synoptic scale limited area model, see Undén [27], are interpolated horizontally in space. A dynamical interpretation model, Danard [8], is utilized to derive the first guess field for the wind component analysis. Optimum interpolation relies on statistical structure functions, e.g. in the form of spatial auto-correlations, determined from historical time series of the data. Since such time series of observed minus first guess data were not available, sensitivity studies have been carried out in order to optimize the system in terms of the first guess error statistics and other tuning parameters.

Basic requirements on the meso-γ analysis scheme, for the nowcasting and very short range forecasting point of view, are described in section 2 of this report, followed by a decription of the mesoscale automatic network of stations in section 3. The analysis methods are described in section 4 while results from evaluations and sensitivity studies, carried out in order to optimize these methods, are described in section 5.

The meso-γ analysis scheme has recently attained increasing interest for air pollution applications. For this purpose it is necessary to determine some parameters which are governing boundary layer dispersion processes. The basis is the meso-γ scale analysis of meteorological parameters. Two methods for determining these dispersion parameters have been compared. Results from this comparison are presented in section 6. Finally an example of utilizing the meso-γ scale analysis fields for an air pollution dispersion experiment is presented in section 7.

Summary and conclusions are given in section 8.

2 Requirements

The mesoscale network of automatic weather stations within the PROMIS project was established for several purposes. Primarily, it was intended as a research tool for the study of mesoscale weather systems and mesoscale modification of larger scale weather systems due to the complicated distribution of land, sea and surface orography within the PROMIS area. Examples of other potential applications for the data from the mesoscale network are:

1. Calibration of radar precipitation measurements by the use of in-situ precipitation measurements at some of the automatic station sites.
2. Forecasting of convective clouds and precipitation by the aid of low level convergence patterns determined from the wind observations in the mesoscale network.
3. Nowcasting and very short range forecasting for local customers, e.g. road authorities, farmers and airport services.
4. Mesoscale input for air pollution models and climatological investigations.
5. Determination of the statistical structures of various meteorological parameters to be used for optimization of future operational observation networks.

For several of these applications, it was considered advantageous to do a pre-processing of the observed data from the mesoscale network by applying automatic quality control checks and by doing objective analysis (spatial interpolation) of the data to a regular grid. For determination of the grid resolution, it was necessary to consider the main physiographic features in the area, e.g. the coastline including some large islands and the bay of Bråviken, the large inland lake Vättern and the hilly area of Kolmården. It was therefore decided to use a grid resolution of 5 km, although the mean distance between the stations in the mesoscale network is as large as 30 km. Since physiographic data are used in the objective analysis procedures, the analysis should not be considered only as a pure spatial interpolation but also as a diagnosis and interpretation tool.

As regards the selection of parameters to be analysed, wind was considered most essential due to the need for determination of convergence patterns mentioned above. In addition, the thermodynamic parameters, temperature

and humidity, were considered necessary for initialization of nowcasting and short range forecasting models. It was not considered relevant to analyse surface pressure since the measurement errors are very large in comparison with the meso-γ scale gradients and, perhaps more important, there were no specific needs for meso-γ scale surface pressure analysis fields.

3 Observations

The PROMIS meso-γ analysis grid covers an area of approximately 265×265 km^2, with the SMHI in Norrköping close to the center, see figure 1. The analysis grid is a rotated lat/long grid with the geometrical north pole positioned at latitude 30° North and longitude 180° West. The grid has a resolution of 0.05 degrees in latitude and longitude, corresponding to ~5.6 km, and contains 47×47 (2209) gridpoints.

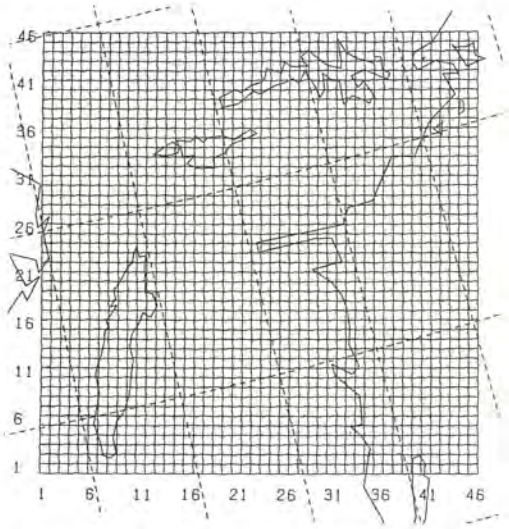

Figure 1: The PROMIS meso-γ analysis area.

A meso-β scale analysis system has been operational for some years at SMHI, Andersson et al [1]. This system utilizes a conventional observation network and operates over an area covering Scandinavia with a resolution of 0.2 degrees.

One of the objectives of the PROMIS project is to see how a completely automatic observation network could be used in an operational forecasting service. For this purpose a network of 40 automatic observation stations was established within the PROMIS area, see figure 2. These stations are primarily reporting temperature, wind and humidity with a frequency of 2–4

reports/hour. In addition there are 25 regular synoptic observation stations giving reports every third hour. Among these synoptic stations 10–15 also give hourly reports (depending on the time of the day). The meso-γ analysis system utilizes all these observations.

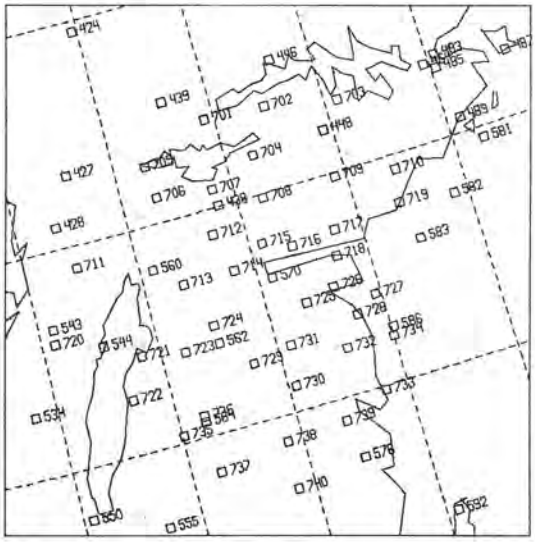

Figure 2: The observation network in the meso-γ analysis area. Stations with number 701–740 are the automatic observing stations, the others are synoptic stations.

4 Analysis methods

4.1 Temperature

The analysis of the 2 metre temperature field is performed with a 2-dimensional uni-variate statistical interpolation technique.

The spatial correlation of the first guess error is represented by a series of zero order Bessel functions:

$$\beta(r) = \sum_{i=1}^{n} A_i J_0(z_i \frac{r}{R})$$

The correlation function used was derived from empirical correlations of observation-climatology based on 5 years data from the Swedish synoptic network.

Looking at the horizontal variability of the screen level temperature and humidity, it is quite obvious that these are highly dependent on the underlying topography. This is also apparent when looking at empirical spatial correlations of the temperature, Andersson et al [1].

From the spatial correlation pattern it is clear that the observed anisotropy, to a large degree, is influenced by the land/sea contrast. To describe this anisotropy we are utilizing a *coastclass modified* structure function for representing the spatial correlation of the first guess errors. So far only the 2 metre temperature is treated in this way. We are using the isotropic spatial correlation functions with a modification based on a coastclass classification of each gridpoint and each station within the analysis area, in the following way:

$$\mu(i,j) \;=\; \alpha(class_i, class_j) * \beta(r_{i,j})$$

where $\beta(r_{i,j})$ is the isotropic distance dependent correlation function and $r_{i,j}$ is the distance between points i and j. The function α is discrete and depends on the coastclasses of the points i and j. The values of this function have been tuned by analysis experiments. Actual values of α are tabulated in table 1.

Figure 3 shows the coastclasses of the observation stations and the gridpoints within the meso-γ analysis area.

There are also other reasons for anisotropy of the temperature field, but these have not been considered when modelling the first guess error correlations.

	1 Inland	2 Near coast	3 Coast	4 Inland lake	5 Sea
Inland	1.0	0.95	0.88	0.88	0.80
Near coast		1.0	0.95	0.95	0.88
Coast			1.0	0.95	0.95
Inland lake				1.0	0.95
Sea					1.0

Table 1: The values of the 'anisotrophic' part of the correlation function, $\alpha(class_i, class_j)$, as a function of coastclasses.

4.1.1 Temperature first guess field

As first guess field for the temperature analysis a short range forecast from the SMHI operational limited area model is used.

In the interpolation of this firdt guess field to the denser meso-γ grid we make use of the gridpoint coast classification. When interpolating to a gridpoint that e.g. is a sea-point we only use surrounding gridpoints that also are sea-points in the coarser grid. By this we maintain the (possibly existing) temperature gradient across a coast even on the finer resolution grid. Hence, temperature gradients across a coast line are better represented by the first guess field than they would have been had a simpler interpolation technique been used.

4.2 Humidity

The analysis of the humidity field is performed with 2-dimensional univariate statistical interpolation.

The spatial correlation functions for the computation of the first guess error covariances are represented by a series of isotropic zero-order Bessel-functions.

As first guess field for the humidity analysis a short-range (3,6 or 9 hour) forecast from the SMHI LAM is utilized.

4.3 Wind

A mesoscale analysis of a near surface wind field has to account for the divergence of the wind field due to e.g. topography, momentum and heat fluxes close to the ground.

In the present analysis scheme the wind analysis has the following characteristics:

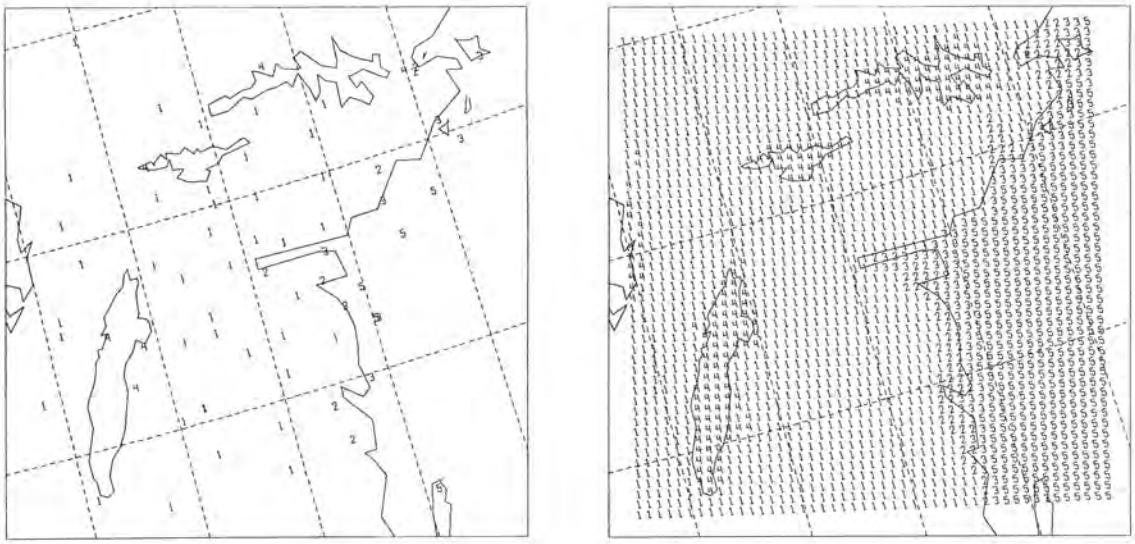

Figure 3: Classification of observing stations (left) and gridpoints in relation to land/sea

- a first guess field is generated by a dynamic simulation of the wind field.
- an optimal interpolation (O/I) technique is used.
- the analysis is accounting for the divergence of the wind field first guess errors.
- the selection of observations is based on the box method.

In the following we discuss these features.

4.3.1 First guess wind field.

The first guess wind field used is obtained by a dynamic simulation of the surface wind. A one-layer primitive equation model, described by Danard [8] is used. Several attempts have been done to tune this model (see section 5.3) in order to get the best fit to observations. It turned out that the model is most sensitive to the surface characteristics and less sensitive to thermodynamical effects. The model is therefore less useful to get e.g. seabreeze patterns not descibed already in the first guess field.

4.3.2 Mathematical formulation of the wind analysis.

The concept of optimum interpolation incorporates a knowledge of the statistical structure of the errors of a first guess field and the errors of the

observations, and their spatial variations. In order to include the divergence in the analysis of the wind field we follow Daley [7] and apply a formulation of the first guess errors of the wind components in terms of a non-divergent part (streamfunction) and a divergent part (velocity potential):

$$u = -\frac{\partial \psi}{\partial y} + \frac{\partial \chi}{\partial x} \tag{1}$$

$$v = \frac{\partial \psi}{\partial x} + \frac{\partial \chi}{\partial y} \tag{2}$$

were ψ is the streamfunction , χ is the velocity potential, and u and v are the wind components of the first guess errors.

If we assume that the spatial covariances of the streamfunction and the velocity potential errors are isotropic and homogenously distributed, and furthermore assume that the non-divergent and divergent part of the errors are uncorrelated, we arrive at the following expressions

$$\begin{aligned} \langle \psi, \psi \rangle &= \overline{\psi^2} F(r) \\ \langle \chi, \chi \rangle &= \overline{\chi^2} G(r) \\ \langle \psi, \chi \rangle &\equiv 0 \end{aligned} \tag{3}$$

where $\overline{\psi^2}$ and $\overline{\chi^2}$ are the variances of ψ and χ, and where $\langle \ , \ \rangle$ stands for the covariance. The functions $F(r)$ and $G(r)$ are the isotropic correlation functions of ψ and χ respectively, and they are only depending on the distance, r.

The spatial covariances of the first guess wind component errors will then be

$$\begin{aligned} \langle u, u \rangle &= -(\overline{\psi^2} \frac{\partial^2 F}{\partial y \partial y} + \overline{\chi^2} \frac{\partial^2 G}{\partial x \partial x}) \\ \langle v, v \rangle &= -(\overline{\psi^2} \frac{\partial^2 F}{\partial x \partial x} + \overline{\chi^2} \frac{\partial^2 G}{\partial y \partial y}) \\ \langle u, v \rangle &= (\overline{\psi^2} \frac{\partial^2 F}{\partial x \partial y} - \overline{\chi^2} \frac{\partial^2 G}{\partial x \partial y}) \end{aligned} \tag{4}$$

As the correlations tends to zero at large separations it is reasonable to pose expansions of the unknown functions F and G in terms of cylindrical harmonics (i.e. Bessel functions) defined by

$$\sum_{i=1}^{n} A_i J_0(k_i r) \qquad , k_i = \frac{z_i}{R}$$

where z_i are the zeros of the first order Bessel function, J_1, and R is a distance scaling factor.

If we assume that the variances of the first guess errors of u and v are equal and that the structure functions F and G have the same shape it is possible to express the correlation functions as

$$\begin{aligned}
\mu(u,u) &= \frac{r_x^2}{r^2}(\gamma_\psi \mu_{lon} + \gamma_\chi \mu_{tra}) + \frac{r_y^2}{r^2}(\gamma_\psi \mu_{tra} + \gamma_\chi \mu_{lon}) \\
\mu(u,v) &= \frac{r_x^2}{r^2}(\gamma_\psi \mu_{tra} + \gamma_\chi \mu_{lon}) + \frac{r_y^2}{r^2}(\gamma_\psi \mu_{lon} + \gamma_\chi \mu_{tra}) \\
\mu(u,v) &= \frac{r_x r_y}{r^2}((\gamma_\psi + \gamma_\chi)(\mu_{lon} - \mu_{lon})) \\
\mu(u,v) &= \mu(v,u)
\end{aligned} \tag{5}$$

were r_x and r_y are the distances, in the x- and y-directions between the two points for which $\mu(u,v)$, $\mu(v,v)$ and $\mu(u,v)$ are calculated. The entities γ_ψ and γ_χ are the fractions of the first quess vector wind error variance arising from the non-divergent and divergent part, respectively. Finally, μ_{lon} and μ_{tra} are defined by

$$\begin{aligned}
\mu_{lon} &= \frac{1}{\beta r}\sum_{i=1}^{n} A_i k_i J_1(k_i r) \\
\mu_{tra} &= \frac{1}{\beta}\left[\sum_{i=1}^{n} A_i k_i^2 J_0(k_i r) + \frac{1}{r}\sum_{i=1}^{n} A_i k_i J_1(k_i r)\right] \\
\beta &= \frac{1}{2}\sum_{i=1}^{n} A_i k_i^2
\end{aligned} \tag{6}$$

where k_i is defined as above.

The approximate solutions for μ_{lon} and μ_{tra} may be found by a least square fit of the coefficients on the right hand side of equation (6) to empirical velocity correlation data. In the present study we have used coefficients A_i as derived for synoptic scales by Hollingsworth and Lönnberg [11], while we have tried to tune the scheme for the mesoscale by adjusting the distance scaling factor R (see below).

4.3.3 Box method.

The objective analysis using an optimal interpolation technique can be compressed into the equation, $a_n = \mathbf{C}^t\mathbf{o}$, where a_n is the analysed deviation from a first guess field at an analysis point n, o is a set of observed deviations

from the first guess field in the neighbourhood of the analysis point and $\mathbf{C}$ is a vector consisting of a number of weights giving the contribution of each observation to the analysed quantity. From the theory of statistical interpolation the weights are found by solving the equation system

$$(\underline{\mathbf{P}} + \underline{\mathbf{D}})\mathbf{C} = \mathbf{P}_n \tag{7}$$

where $\underline{\mathbf{P}}$ and $\underline{\mathbf{D}}$ are the first guess error covariance matrix and the observational error covariance matrix for the observational points, respectively. $\mathbf{P}_n$ is a vector with the first guess error covariances between the observational points and the analysis point n.

Generally a limited number of observations could, for computational reasons, be used to evaluate each gridpoint value, demanding an observational selection technique in order to use the limited number of observations in an optimal way.

A problem arising from a local selection technique is that different sets of observations may be contributing to adjacent analysis gridpoints. This could especially for wind analysis cause serious errors if the observations are inhomogenously distributed in space, giving rise to e.g. fictitious divergence patterns.

A way of solving this problem is to use a so called box method, see Lorenc [18]. The analysis area is then divided into boxes, where the set of observations, contributing to the analysed values, is the same for all gridpoints within each box. Fortunately the meso-γ analysis area is small enough for the whole analysis area to be regarded as a single box. The analysis procedure is then simplified in the following way.

$$\mathbf{a} = \underline{\mathbf{P}_n}\mathbf{U} \tag{8}$$

where $\mathbf{a}$ is a vector containing all the analysis values within the box, $\underline{\mathbf{P}_n}$ is the first guess error covariance matrix with respect to observational and analysis points, and $\mathbf{U}$ is the solution of the linear system of equations

$$(\underline{\mathbf{P}} + \underline{\mathbf{D}})\mathbf{U} = \mathbf{o} \tag{9}$$

where $\mathbf{o}$ now is all the observations available.

The equation systems (8) and (9) then forms the set of equations for the O/I box method.

4.4 Quality control

An important element of all numerical analysis schemes is the quality control of the observations that are going to be used in the analysis.

The quality control of the observations in the meso-γ scale analysis consists of a gross error check and a horisontal consistency check.

The gross error check compares the observation increments, f_o^{inc}, (observation - first guess) with pre-specified limits ,TOL. If

$$abs(f_o^{inc}) < TOL$$

is satisfied, the observation is accepted, if not it is rejected.

TOL is constant and equal to 15.0 degrees for the temperature analysis.

In the wind analysis, the wind speed observation increment is compared with TOL $= 15.0 + F \cdot 10.0$, where F is a sinosoidal function dependent on the month. The value of F is 0.0 for July and 1.0 for January, thus allowing greater observation increments during the winter season.

No gross error check is applied for humidity.

During the horisontal consistency check, each observation increment is compared with an analysis increment, f_{na}^{inc}. The analysis increment is obtained by optimal interpolation to the position of the observation using the surrounding observation increments, but excluding the observation to be checked. The selection of influencing observations is done by the same selection algorithm that is used in the final analysis to the gridpoints. See Andersson et al [1]. (Also for the wind, a local data selection is done)

The observation increment is compared with the analysis increment. If

$$abs(f_{na}^{inc} - f_o^{inc}) \leq TOL1$$

the observation is considered correct, and if

$$TOL1 < abs(f_{na}^{inc} - f_o^{inc}) \leq TOL2$$

the observation is considered suspect. If

$$abs(f_{na}^{inc} - f_o^{inc}) > TOL2$$

it may be that the observation is erroneous, but there is also a possibility that one (or more) of the utilized observations in the vicinity is erroneous. In this case a new analysis increment, with one of the selected observations

excluded, is computed and the check it repeated. If the observation still fails to be accepted, the procedure is repeated with another observation excluded until all selected observations have been excluded or until the observation is accepted. Only if the observation every time fails to be accepted, the observation is rejected, else it is accepted.

For the temperature analysis we have

$$TOL1 = MAX(TOLMIN, 3.0 \cdot \sigma_{Terr})$$

$$TOL2 = MAX(1.25 \cdot TOLMIN, 4.0 \cdot \sigma_{Terr})$$

where σ_{Terr} is the estimated standard deviation of the interpolation error and TOLMIN is a minimum value (3.0, 4.0, 5.0, 6.0 or 7.0 depending of the time of the day and the coastclass classification of the observing station).

The relative humidity is checked against

$$TOL1 = MAX(0.15, 3.0 \cdot \sigma_{Rerr})$$

$$TOL2 = MAX(0.20, 4.0 \cdot \sigma_{Rerr})$$

where σ_{Rerr} is the estimated standard deviation of the interpolation error.

Wind speed observation increments, $\sqrt{(u_o^{inc})^2 + (v_o^{inc})^2}$ are checked against the tolerances

$$TOL1 = 5.0 \cdot VAR$$

$$TOL2 = 9.0 \cdot VAR$$

where VAR = (estimated variance of the interpolation error of the u-component + estimated variance of the interpolation error of the v-component + variance of the observation error).

It should also be mentioned that conventional internal consistency checks and time consistency checks are carried out during the pre-processing of the observations.

5 Evaluations and sensitivity studies

At the time of writing no statistics were available on the deviations of observations from first guess, and sensitivitity studies were therefore designed to look at the impact on an analysis from different choises of analysis parameters.

By varying the standard deviation of the first guess errors, σ^{fg}, while keeping the standard deviation of the observational errors, σ^{obs}, constant the first guess field and the observations will be differently weighted together when forming the final analysis.

It might be tempting to put as large an emphasis on the observations as possible, but such a choice can be devastating for the analysis since observational errors might be drawn for. By comparing the analysis with observations not included in the analysis itself it is possible to arrive at a proper signal-to-noise relation σ^{fg} / σ^{obs}

In the sensitivity studies we also looked upon the impact of different values of the characteristic lengthscale on the analysis by changing the distance scaling factor , R, of the correlation functions,

$$\beta(r) = \sum_{i=1}^{n} A_i J_0(z_i \frac{r}{R})$$

By decreasing R we try to analyse smaller scale features present in the observations.

In the wind analysis we first looked upon how well the dynamic model could provide a first guess wind field to be used in the analysis. We also examined the impact of different fractions of the divergent and non-divergent part in the wind vector correlation functions.

For the sensitivity studies we created a test data base covering two periods, each of a duration of two weeks, during the winter and spring of 1988. The first period was in March (8 - 21) and the second in May (8 - 23).

The analysis tests were performed every 3:rd hour. Excluding some analysis hours due to missing data, the test period covered 107 analyses. The evaluation was done by excluding 5 weather stations from the analysis, to be used as independent reference observations. The locations of these stations are shown in figure 4.

Statistics from the differences between the excluded observations and the resulting analyses were used to evaluate the sensitivity to different choices of analysis parameters.

Figure 4: Observations excluded in the test analysis

5.1 Temperature

In the analysis of temperature a value of 1.0 K was used for the standard deviation of the observational error, σ_T^{obs}, and in the different analysis tests the first guess error standard deviation, σ_T^{fg}, was varied between 2.0, 4.0 and 6.0 and the distance scaling factor, R, between 150 , 250 and 350 km.

The statistics (se table 2) showed over all small differances for different values of σ_T^{fg} and R. The results pointed out, however, a slight improvement of the analysis with a small σ_T^{fg} and a greater R. This means that even on this small scale, the meso-γ scale, the temperature observations, to a large extent, are influenced by even smaller features than the station network can represent. The best fit choice of σ_T^{fg} and R was 2.0 K and 350 km, respectively.

5.1.1 Example of temperature analysis

An example of a temperature analysis is given in figure 5. The corresponding observations at the same time are shown in figure 6.

5.2 Humidity

In the analysis of relative humidity a value of 5% was used for the standard deviation of the observational error, σ_R^{obs}, and in the different analysis runs the first guess error standard deviation, σ_R^{fg}, was varied between 5 , 10 and

	bias $T_{obs} - T_{na}$	standard deviation $T_{obs} - T_{na}$	correlation T_{obs}, T_{na}
R=150, σ_T^{fg}=2.0	0.07	1.24	0.991
R=150, σ_T^{fg}=4.0	0.10	1.39	0.988
R=150, σ_T^{fg}=6.0	0.12	1.47	0.987
R=250, σ_T^{fg}=2.0	0.05	1.16	0.991
R=250, σ_T^{fg}=4.0	0.13	1.22	0.990
R=250, σ_T^{fg}=6.0	0.16	1.28	0.989
R=350, σ_T^{fg}=2.0	0.03	1.15	0.991
R=350, σ_T^{fg}=4.0	0.10	1.15	0.991
R=350, σ_T^{fg}=6.0	0.16	1.19	0.990

Table 2: Statistics from the sensitivity studies of the temperature analysis. T_{obs} is a temperature observation from an independent reference station and T_{na} is the analysed value interpolated to the observing station.

15% and the distance scaling factor, R, between 150 , 250 and 350 km. The result of the sensitivity test can be seen in table 3.

5.2.1 Example of humidity analysis

An example of a humidity analysis is given in figure 7. The observations at that time are shown in figure 8 and the observed relative humidities are plotted in figure 9.

5.3 Wind

5.3.1 First guess wind field

A first guess wind field is obtained diagnostically by a dynamic simulation of the surface wind. A one-layer primitive equation model is used with the purpose to find a quasi-stationary balance in terms of the pressure and temperature fields, taking frictional, orographic and stability effects into account, Danard [8]. The pressure field used is obtained by interpolation from an operational meso-β scale analysis, Andersson et al [1], while the meso-γ scale temperature field is obtained by methods described in this paper. The model is initialized by an Ekman wind balance determined for each gridcell.

Several tests have been performed to tune the diagnostic model in order

Figure 5: Temperature analysis at 12 UTC 15/5 1988. Isolines for the temperature are at 1.0 intervals.

to get the best fit to observational data. The tests have been done by modifying the roughness field which was estimated from orography variance, surface type and vegetation type.

The modifications were designed by looking at the bias of the difference between the simulated and observed windspeeds and winddirections. The tuning gave contradictory results, however. A modification giving an improvement for the testperiod in late winter (March) deteriorated the simulations for the spring data (May). It was also found that the model is not capable of describing thermal effects as seabreeze. We also compared the initial wind field, the Ekman wind (the starting point for the dynamic model) with the observations. The initial wind fields appear to give the same scatter around the observations as the dynamic model, see figure 10 and figure 11. From this we concluded that the dynamic model had no skill over the initial wind field. Some further tests were performed in order to tune the initial wind field, but did not work out all too successfully.

It was finally concluded that the initial wind field (Ekman wind balance) is sufficient as a first guess for the analysis until a model more capable of describing mesoscale effects is available.

5.3.2 Divergence

In a number of test runs we investigated the impact on the wind analysis of different values of the parameters γ_χ and γ_ψ, discribing the relative contri-

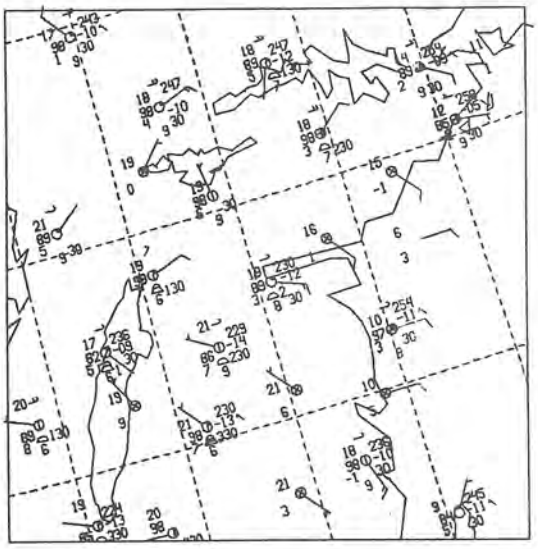

Figure 6: Observations at 12 UTC 15/5 1988.

butions of the divergent part and the non-divergent part of the wind vector correlation functions, respectively. We ran the wind analysis with the value of γ_χ varying between 0.0, 0.05, 0.10, 0.15, 0.20, 0.25 and 0.30, interpreted as strictly non-divergent analysis to a mix of divergence and non-divergence of 0.3 and 0.7, respectively.

The results, see table 4, indicated an improvement of the analysis when the divergent part of the wind was included. The great improvement when including a divergent part is in the wind field pattern, which is clearly illustrated in figure 14 and figure 15. On the other hand, the evaluations did not show any further improvements when γ_χ was increased from 0.05 to 0.30.

The values of the parameters γ_χ and γ_ψ were therefore set to 0.10 and 0.9, respectively, in the operational meso-γ analysis system.

5.3.3 Sensitivity to first guess error and influence radius

In the analysis of the wind components a value of 1.5 m/s was used for the standard deviations of the observational error, σ_u^{obs} and σ_v^{obs}, and in a number of test runs we first varied the first guess error standard deviations, σ_u^{fg} and σ_v^{fg}, between 2.5 , 5.0 and 10.0 m/s. The results of this sensitivity study can be seen in table 5. The tests showed that σ^{fg}=10.0 was too large a value with σ^{obs}=1.5 and we decided to use σ^{fg}=5.0 .

We then studied the sensitivity of the wind analysis scheme for different values of the distance scaling factor, R, and let it vary between 150 , 250 and 350 km. The results of this study can be seen in table 6. In the operational

	bias $R_{obs} - R_{na}$	standard deviation $R_{obs} - R_{na}$	correlation R_{obs}, R_{na}
R=150, σ_R^{fg}= 5.0	-0.90	9.00	0.869
R=150, σ_R^{fg}=10.0	-1.31	6.99	0.923
R=150, σ_R^{fg}=15.0	-1.22	7.11	0.920
R=250, σ_R^{fg}= 5.0	-1.76	7.25	0.917
R=250, σ_R^{fg}=10.0	-1.79	7.00	0.923
R=250, σ_R^{fg}=15.0	-1.77	7.30	0.916
R=350, σ_R^{fg}= 5.0	-1.98	7.54	0.910
R=350, σ_R^{fg}=10.0	-1.94	7.43	0.913
R=350, σ_R^{fg}=15.0	-2.02	7.71	0.906

Table 3: Statistics from the sensitivity studies of the humidity analysis. R_{obs} is an observation of relative humidity from an independent reference station and R_{na} is the analysed value interpolated to the observing station.

use the wind analysis is run with R=250 km.

5.4 Examples of divergence fields

A good example of the ability of the analysis system to describe divergence in the wind field is the situation at 12 UTC on the 15th of May 1988. The observations are shown in figure 12 and indicates a rather week but well-defined convergence zone some 20–30 km from the coast over land.

The first guess wind field used in the analysis, obtained by a dynamic simulation of the surface wind, and its divergence field is shown in figure 13 and it is clear that the convergence zone is not present in this first guess.

The analysis of wind and divergence are shown in figure 14 and it can be seen that the convergence zone is well described. In this analysis run we assumed the divergence parameter γ_χ to be 0.1 in modelling the first guess error covariances.

The corresponding analyses, with the wind considered to be purely rotational in modelling the first guess wind error covariances (γ_χ =0.0), are shown in figure 15.

This shows very clearly the need to model the divergent part of the wind if a good representation of wind and divergence fields on this scale should be possible.

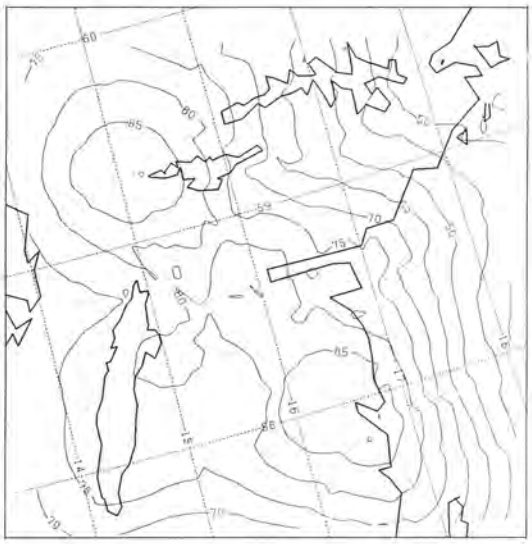

Figure 7: Humidity analysis at 06 UTC 8/5 1988. Isolines for the relative humidity are at 5% intervals.

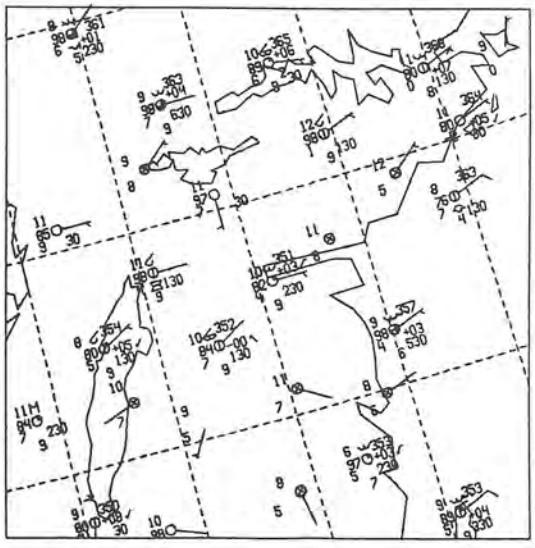

Figure 8: Observations at 06 UTC 8/5 1988.

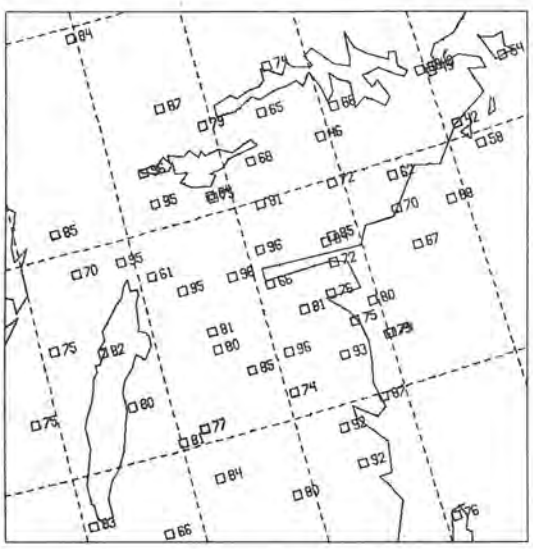

Figure 9: Observations of relative humidity at 06 UTC 8/5 1988.

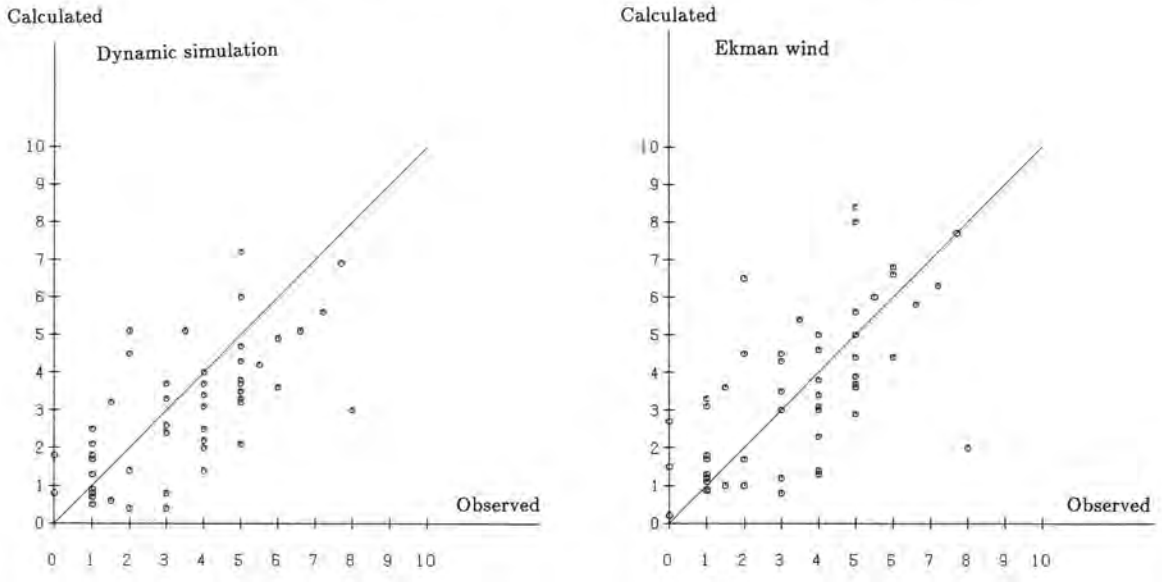

Figure 10: Test results showing simulated versus observed windspeed at an inland station (Norrköping-Bråvalla) for a dynamic model (left) and a Ekman wind used for initialization of the dynamic model (right).

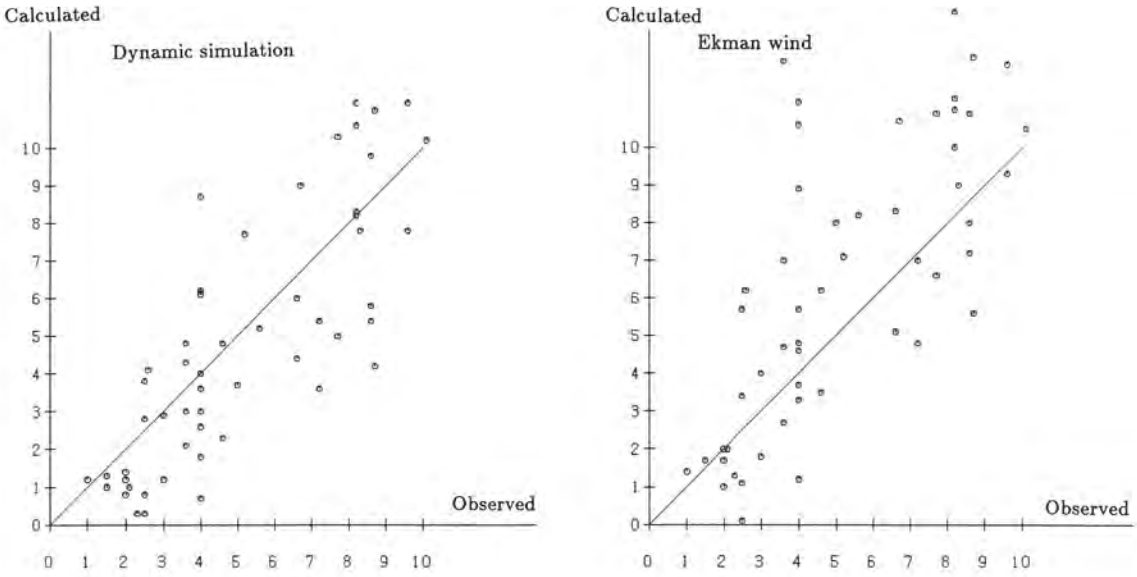

Figure 11: Test results showing simulated versus observed windspeed at a sea station (Harstena) for a dynamic model (left) and a Ekman wind used for initialization of the dynamic model (right).

	bias $u_{obs} - u_{na}$	bias $v_{obs} - v_{na}$	standard deviation $u_{obs} - u_{na}$	standard deviation $v_{obs} - v_{na}$	correlation u_{obs}, u_{na}	correlation v_{obs}, v_{na}
γ_χ=0.0	-0.15	-0.04	1.90	1.85	0.85	0.86
γ_χ=0.05	-0.22	-0.06	1.83	1.68	0.87	0.89
γ_χ=0.1	-0.23	-0.06	1.84	1.69	0.86	0.89
γ_χ=0.15	-0.23	-0.06	1.85	1.69	0.86	0.89
γ_χ=0.2	-0.23	-0.06	1.87	1.70	0.86	0.89
γ_χ=0.25	-0.23	-0.07	1.87	1.70	0.86	0.88
γ_χ=0.3	-0.23	-0.07	1.88	1.70	0.85	0.88

Table 4: Statistics from the sensitivity studies of the divergence. u_{obs} and v_{obs} are observations of the wind components from an independent reference station and u_{na} and v_{na} are the corresponding analysed values interpolated to the observing station.

	bias $u_{obs} - u_{na}$	bias $v_{obs} - v_{na}$	standard deviation $u_{obs} - u_{na}$	standard deviation $v_{obs} - v_{na}$	correlation u_{obs}, u_{na}	correlation v_{obs}, v_{na}
$\sigma^{fg}_{u,v}$= 2.5	-0.18	-0.07	1.87	1.64	0.86	0.89
$\sigma^{fg}_{u,v}$= 5.0	-0.22	-0.07	1.83	1.65	0.87	0.89
$\sigma^{fg}_{u,v}$=10.0	-0.23	-0.06	1.88	1.85	0.85	0.86

Table 5: Statistics from the sensitivity studies of the wind analysis with different values of the standard deviations of the first guess error for the wind components, σ^{fg}_u and σ^{fg}_u.

	bias $u_{obs} - u_{na}$	bias $v_{obs} - v_{na}$	standard deviation $u_{obs} - u_{na}$	standard deviation $v_{obs} - v_{na}$	correlation u_{obs}, u_{na}	correlation v_{obs}, v_{na}
R=150	-0.25	-0.04	1.91	1.91	0.85	0.85
R=250	-0.22	-0.07	1.83	1.65	0.87	0.89
R=350	-0.18	-0.07	1.92	1.59	0.85	0.90

Table 6: Statistics from the sensitivity studies of the wind analysis with different values of the distance scaling factor, R.

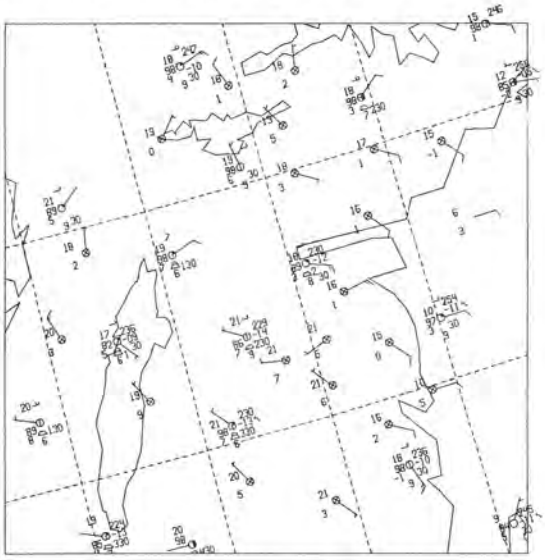

Figure 12: Observations at 12 UTC 15/5 1988.

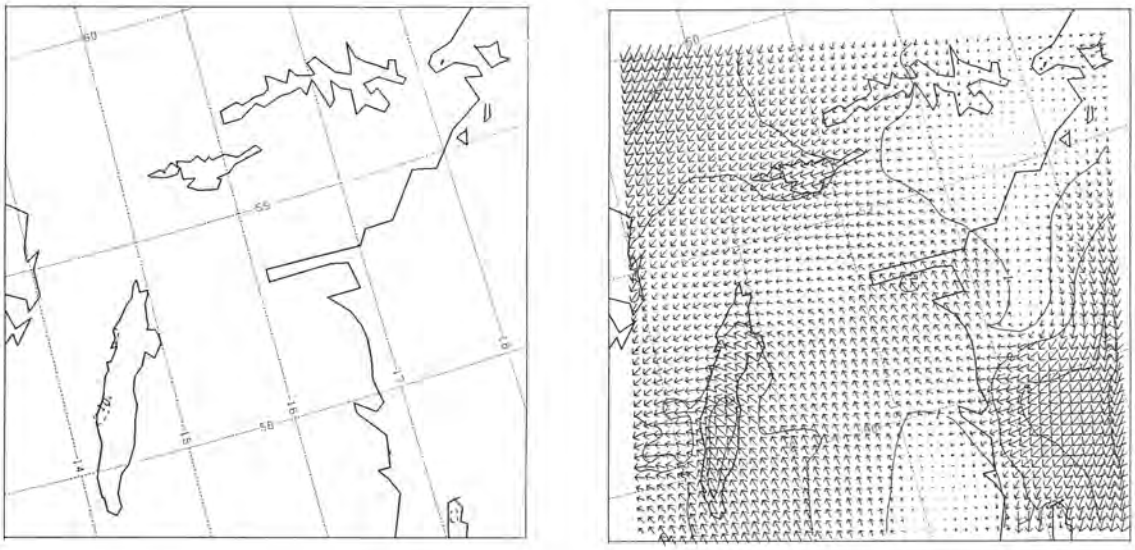

Figure 13: First guess wind (right) and divergence (left) fields. The unit of the divergence is $10^{-5} \cdot s^{-1}$.

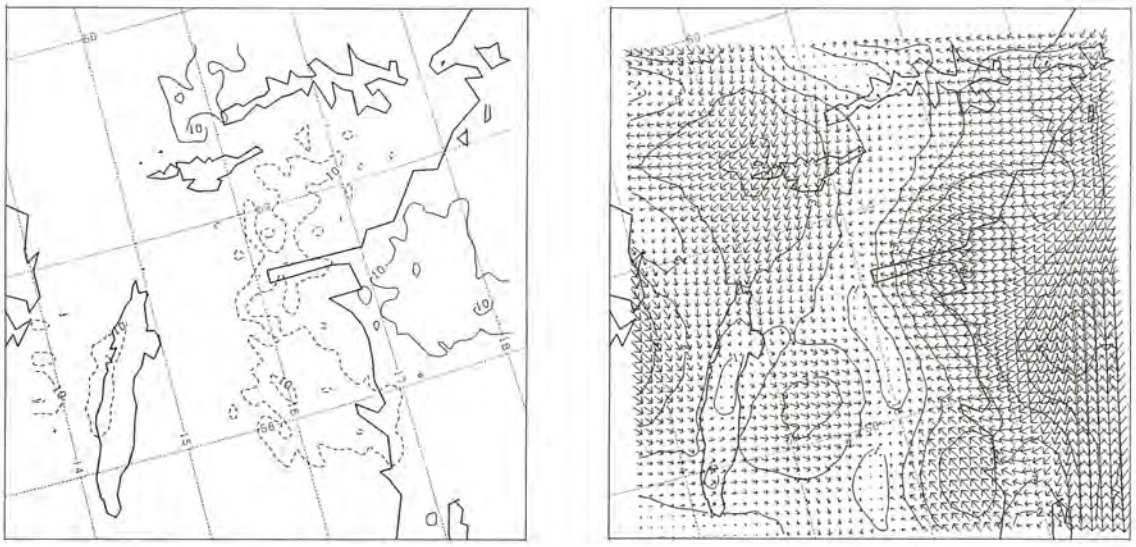

Figure 14: Wind (right) and divergence (left) analysis with γ_χ =0.1

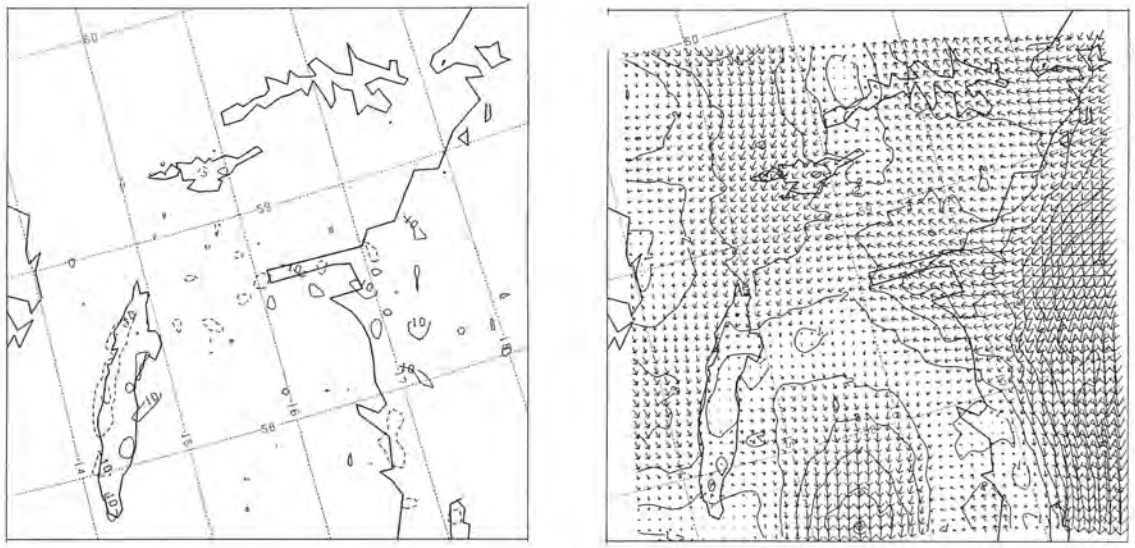

Figure 15: Wind (right) and divergence (left) analysis with γ_χ =0.0

6 Estimation of boundary layer parameters

6.1 Introduction

The analyses described in previous sections together with analyses of other meterological parameters , described by Andersson et al [1], form a set of routine meteorological data in grid form possible to use for short term weather forecasts and for air pollution models. In order to provide input data for these models, the turbulent state of the atmospheric boundary layer (ABL) has to be determined, and thus it is necessary to use parameterizations in terms of the routine meteorological data avaliable.

Essential parameters which determine the state of the ABL are profiles of wind, turbulence and temperature.

From similarity theory these profiles can be obtained from three primary ABL parameters, H_0 the surface sensible heat flux, τ_0 the surface momentum flux and h the height of the ABL, Monin and Obukhov [20].

Several attempts have been made to parameterize the turbulent surface fluxes of the ABL in terms of routine meteorological data, Berkowicz and Prahm [2], Holtslag and de Bruin [12] and Van Ulden and Holtslag [28].

We have here tested two sets of procedures for different surface types namely

1. Model formulation 1
   (a) Resistance model for rural and forest areas
   (b) Box model for urban areas
   (c) Gradient flux model for water surfaces
2. Model formulation 2
   (a) Modified Priestley-Taylor model for rural, forest and urban areas
   (b) Gradient flux model for water surfaces

The first formulation has been used for several years in air pollution applications at SMHI, Omstedt [23] and Omstedt [24], except for urban areas where the resistance method was used, and it has also been implemented in a short term weather forecast model, Gollvik and Omstedt [15]. The second formulation is based on a work done by van Ulden and Holtslag [28], and has been implemented in a multi layer Air Mass Transformation Model. The method has been further developed according to Holtslag and de Bruin [12] for the nocturnal ABL, although this is not described here.

Here we have made the assumption that the parameterizations, mentioned above, which were developed and evaluated for point measurements, could be generalized to be valid also for meteorological data generated by an objective analysis, and therefore representing gridpoint values with subgrid scale variations eliminated (closely related to a mean value over each gridsquare). An apparent weakness of this assumption is that the parameterizations of e.g. the resistance model and the modified Priestley-Taylor model, are primarily valid for grass covered fairly flat terrain, while we are using the methods for other surface types (although with some modifications) and for more or less complex terrain.

Another assumption is that the surface layer parameters are estimated entirely by the processes within each gridsquare indepentently of adjacent gridsquares. This assumption could be regarded as reasonable for the processes within the surface layer, while the description of processes in the upper part of the ABL has to account for effects as e.g. advection of temperature and turbulence. In order to take this into account to some extent a semi-Lagrangian advection model is used to obtain the depth of the ABL.

For each gridsquare the surface fluxes are evaluated for each of the surface types present in the gridsquare (forest, rural, urban or water surface). The final estimates of the fluxes representing the whole gridsquare are then taken as weighted means of the fluxes from the different surface types according to their fractions of the gridsquare.

6.2 General approach

The energy fluxes close to the ground obey the surface energy balance equation

$$H_0 + \lambda E \;=\; Q^* \,\text{fi}\, G \tag{10}$$

where H_0 is the surface sensible heat flux, λE is the latent heat flux, Q^* is the net radiation and G is the soil heat flux. The right hand side stands for the input energy, and the left hand side the energy supplied or withdrawn from the atmosphere. Several approaches could be found to solve this equation for different surfaces. A brief description of the two different model formulations is given in appendix A.

6.3 Results

To compare the relative merits of the two model formulations, a test period was chosen in the autumn of 1988 (27 to 29 October). During this period a rapid and strong coldfront was passing over the area. The air temperature

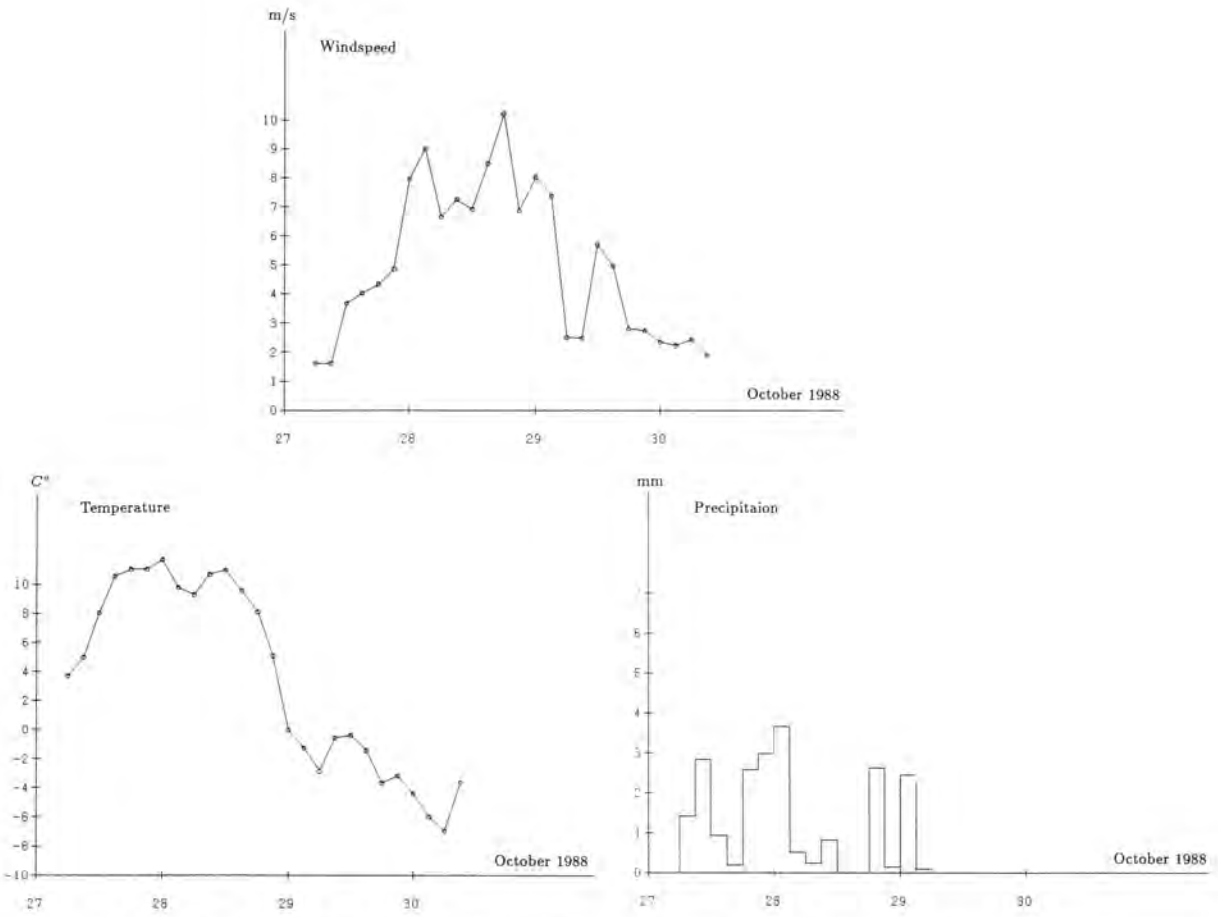

Figure 16: The evolution of wind, temperature and precipitation during the period 27 - 30 October 1988, as analysed by the meso-γ scale analysis in a gridpoint somewhere in the center of the analysis area.

decreased by 12 $°C$ and quite strong winds occured at the time. In figure 16 the evolution of temperature, wind and precipitation are shown. The data presented in these figures are analysis values taken from a center point of the meso-γ analysis area. The period was selected because of this rapid change of airmass, and was considered to be a good test of the performance of the various methods.

The results of the two different model formulations are shown in figures 17, 18, 19 and 20. Gridpoints which are dominated by a single surface type have been selected.

The most apparent differences between the two model formulations are found in forest areas, where the resistance method gives an intense latent heat flux in the morning of the second day of the test period, while the modified Priestley-Taylor model only gives a slight increase in this flux. For urban areas the Priestley-Taylor model gives very similar result as for rural areas with the same model, with dominating negative sensible heat flux. The more simple approach chosen for urban areas in the first model formulation gives on the contrary positive latent and sensible heat fluxes for the whole test period.

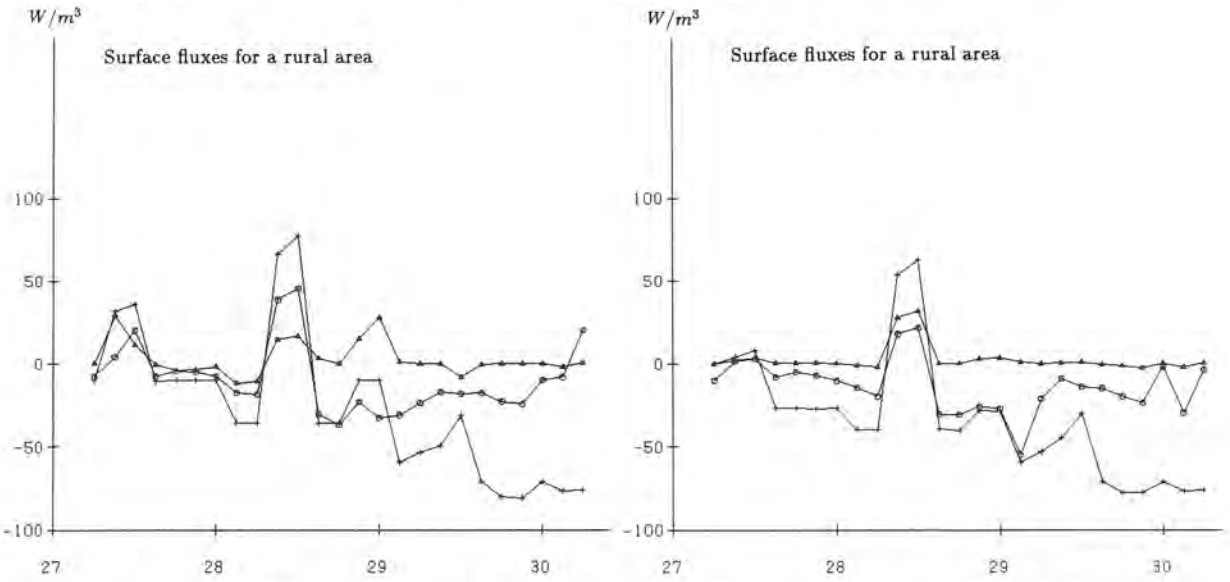

Figure 17: The evolution of the sensible heat flux (.), latent heat flux (Δ) and the net radiation (x), during the period 27 - 30 October 1988, for a rural area calculated by the resistance method (left) and the modified Priestley-Taylor model (right).

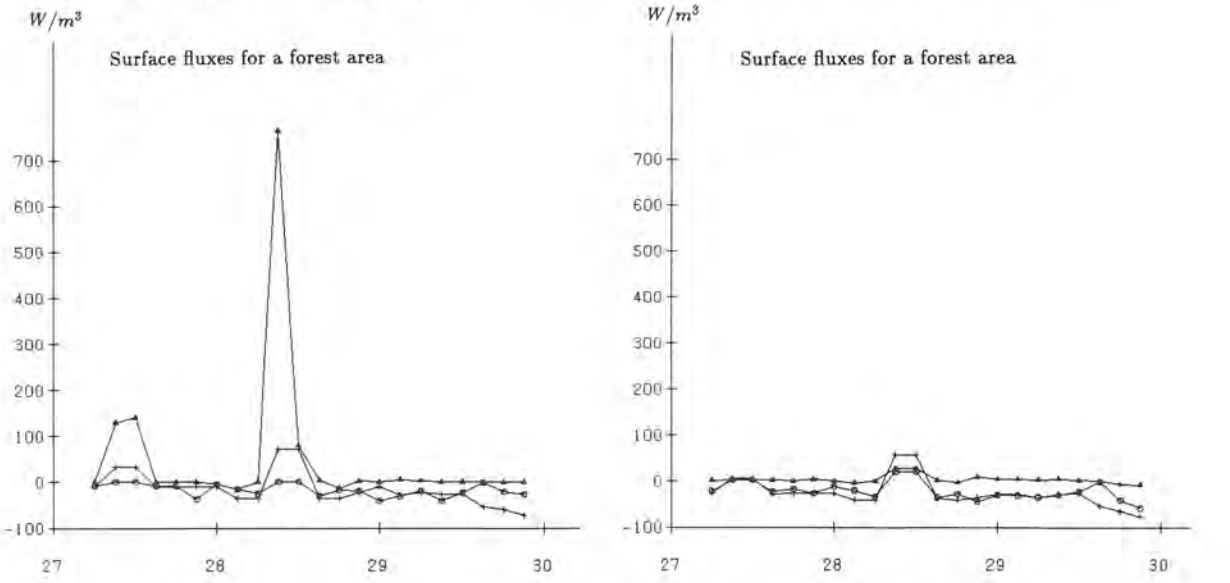

Figure 18: The evolution of the sensible heat flux (.), latent heat flux (Δ) and the net radiation (x), during the period 27 - 30 October 1988, for a forest area calculated by the resistance method (left) and the modified Priestley-Taylor model (right).

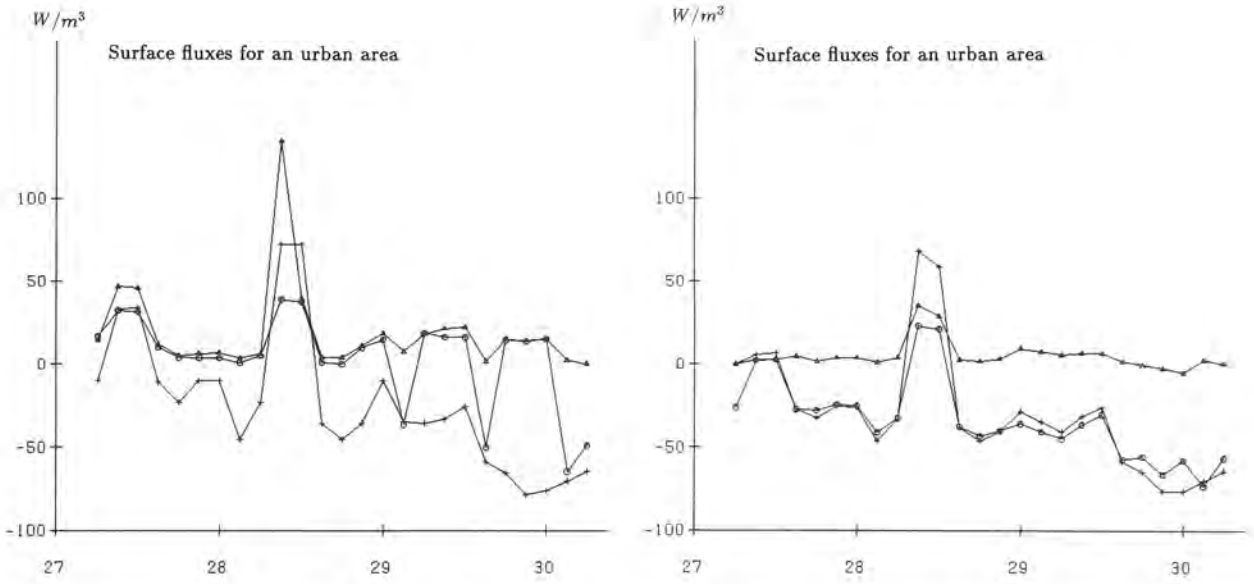

Figure 19: The evolution of the sensible heat flux (.), latent heat flux (Δ) and the net radiation (x), during the period 27 - 30 October 1988, for an urban area calculated by a simple box method (left) and the modified Priestley-Taylor model (right).

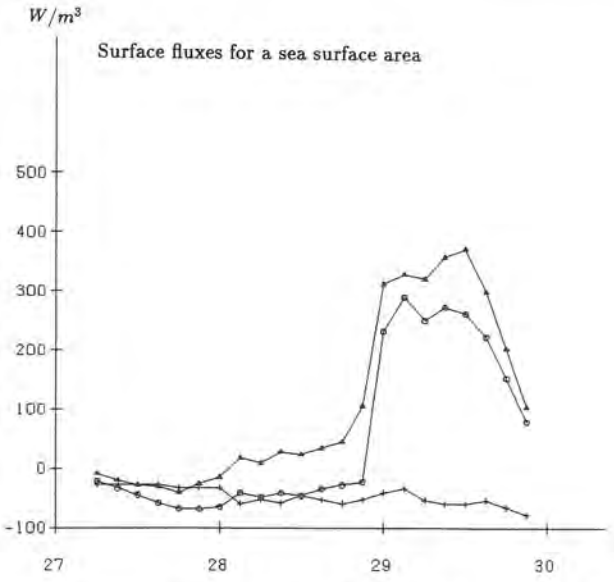

Figure 20: The evolution of the sensible heat flux (.), latent heat flux (Δ) and the net radiation (x), during the period 27 - 30 October 1988, over a sea surface area calculated by a simple bulk approach. Note the rapid response in the fluxes as the airmass changes.

Neither of the two model formulations does, however, respond to the rapid change of airmass as could be expected, except for water surfaces, figure fig 20. For this reason the value of these model formulations has to be questioned. For both model formulations the evolution of the surface temperature is not explicitly described, but included in parameterization schemes primarily validated by data sets without advective situations, de Bruin and Wessel [4]. The methods should therefore not be expected to describe airmass transformations in any detail.

In order to set scores for the two models, calculations of the boundary layer height (ABL) have been compared with radiosonde data from the Bromma station. The boundary layer height is determined by the parameters that comes out from the model formulations tested above. For a full description see Appendix. Input taken from either of the two model formulations gives quite comparable results with a slightly better fit to observed boundary layer height when taking the input from the Priestley-Taylor model. Although, due to the weak response to the airmass shift in both of the model formulations tested, the boundery layer height is underestimated for the first part of the test period.

Calculations have also been performed with observed entities used instead of the analysed equivalent. This means that the gridpoint values are determined by observed instead of analysed input data for the gridsquares that enclose the weather stations selected. The observed entities are therefore assumed to be representative for the weather conditions within the whole gridsquare. A number of 15 routine weather stations have been used in this test.

The results are plotted in figures 22 and 23 for the sensible and latent heat flux, respectively, with the result from observed input data plotted versus the result from analysed input data. Both model formulations are included in the test and results are presented in the figures.

The comparison shows a fairly good one-to-one agreement for low and negative sensible heat fluxes. A larger scatter is apparent for large sensible heat fluxes. These fluxes emerge primarily from sea surfaces where a bulk formulation is used. The main reason for the scatter is the difference between analysed and observed windspeed. The analysed windspeed seems often to be larger than the observed over sea surfaces, giving larger turbulent fluxes.

It could be argued, however, that the analysed wind is more representative for water surfaces than the observed. The observed wind is reflecting the local conditions of the measurement site, which normally is an island. The analysed wind field has on the contrary a structure given by the background field which is taking the mean roughness and stability (within each

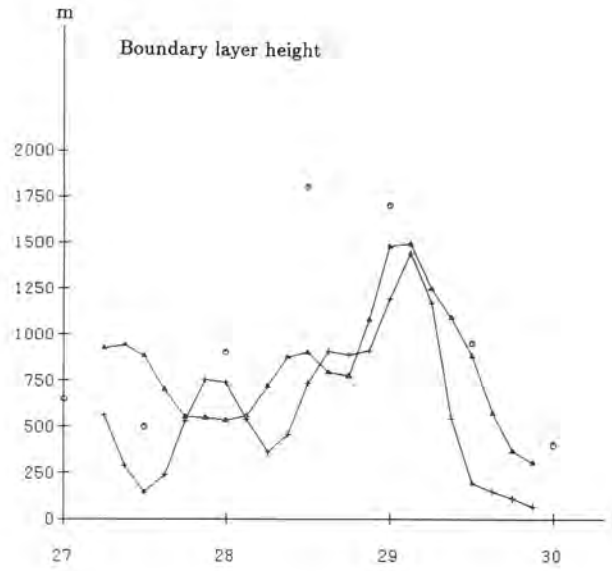

Figure 21: Calculated boundary layer height (solid line) plotted together with observed boundary layer heights (.) at the Bromma radiosonde station, where the boundary layer fluxes used where determined by a) the model formulation 1 (+, basically the resistance method) and b) formulation 2 (Δ, basically the modified Priestley-Taylor model).

gridsquare) and the larger scale pressure gradient, into account.

The plot of the calculated latent heat flux exhibits quite a large scatter. The Priestley-Taylor model gives a doubling of the latent heat fluxes, when using analysed instead of observed input data. The reason for this might be the close relation between the soil moisture and the latent heat flux in the Priestley-Taylor model. The precipitation analysis and the soil moisture treatment will then be cruicial for this model.

The conclusion from the various tests will be that the different boundary layer parameterizations tested, have a limited ability to describe the evolution of the surface fluxes during a rapid airmass transformation. The bulk approach gives in this respect the most realistic result.

The bulk formulation used for water surfaces seems, however, to be quite sensitive to input data. In this case analysed input data is argued to be more representative for sea surface grid squares than pure observed data.

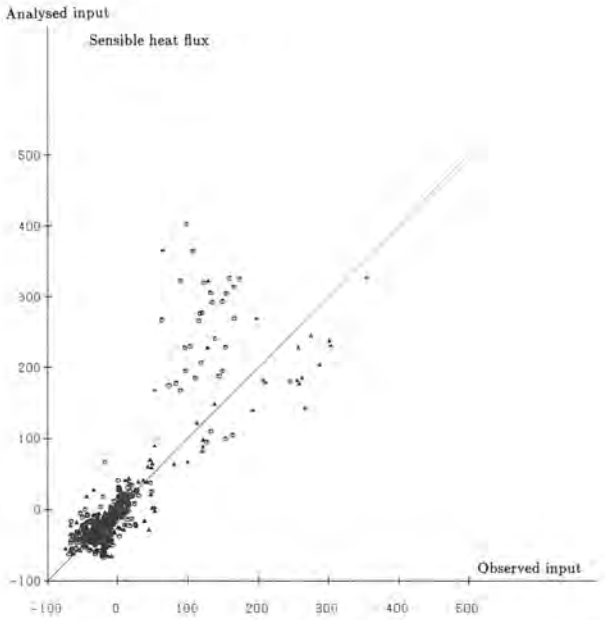

Figure 22: Calculated sensible heat flux with the use of observed versus analysed input data. The data covers the period 27 - 30 October 1988. Both model formulations 1 (Δ) and 2 (.) are plotted.

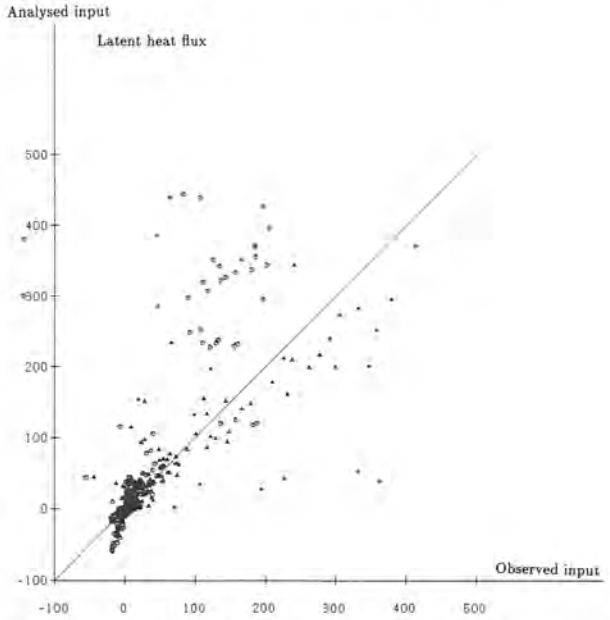

Figure 23: Calculated latent heat flux with the use of observed versus analysed input data. The data covers the period 27 - 30 October 1988. Both model formulations 1 (Δ) and 2 (.) are plotted.

7 An air pollution dispersion application

The analysis of different meteorological and boundary layer parameters offers an excellent tool for air pollution applications. The analysis system has been applied to the southernmost part of Sweden, the Skåne area, to provide a meteorological data set for air pollution assessment studies. A regional scale dispersion model has for this purpose been developed at SMHI, sponsored by Skånes Luftvårds förbund, Persson et al [25].

In order to describe the potential of this type of analysis, a random walk model has been developed. The model is an autoregressive model governed by a non-stationary stochastic process following Yamada et al [29] and Hanna et al [10]. The turbulent structure of the boundary layer is taken into account by parameterization.

One analysis for the Skåne area has been selected as an example. Some of the basic analyses used and the result of the dispersion simulation for a case in the morning of 8 December 1988 are shown in figures 24, 25, 26 and 27.

A nonreactive effluent is emitted into a stable boundary layer inland (over Sjaelland), and transported into a convective boundary layer offshore. When crossing the coastline an apparent fumigation is taking place,as shown in the cross-image of the plume in figure 27. As the effluent is subject to a vertical spread, it will be affected by different winds at different levels in the boundary layer. Some particles will follow paths mainly governed by the surface wind and be transported into a stable boundary layer over the very southern part of Sweden. Other particles will remain in the convective boundary layer over the sea. A steady-state is assumed, although this is not quite correct, and the particles are followed during a time period of twelve hours.

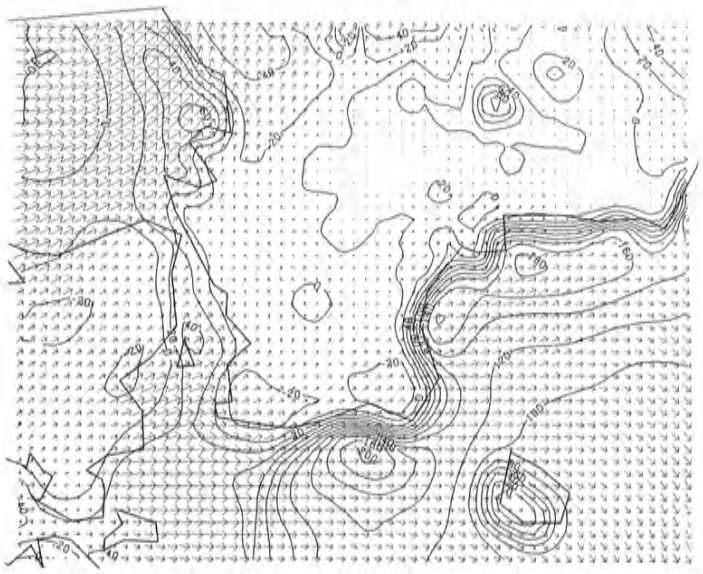

Figure 24: Meso-γ analyse of near surface wind and calculated sensible heat flux

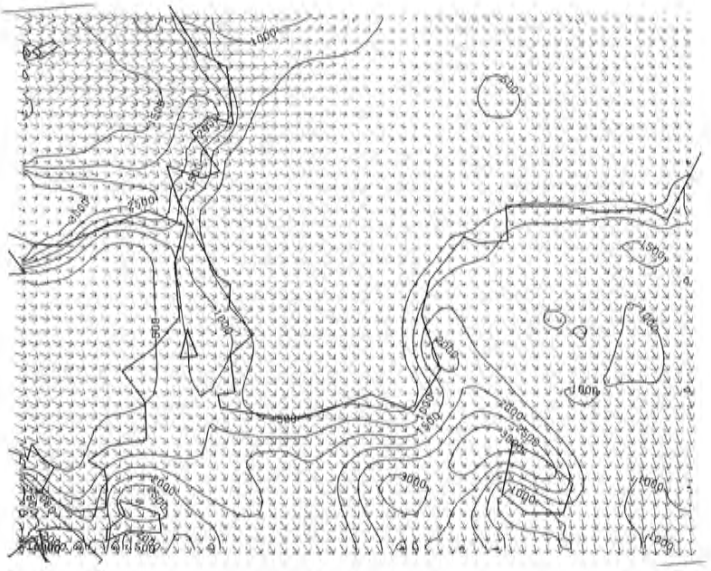

Figure 25: Meso-γ analyse of 850 hPa wind and calculated boundary layer height

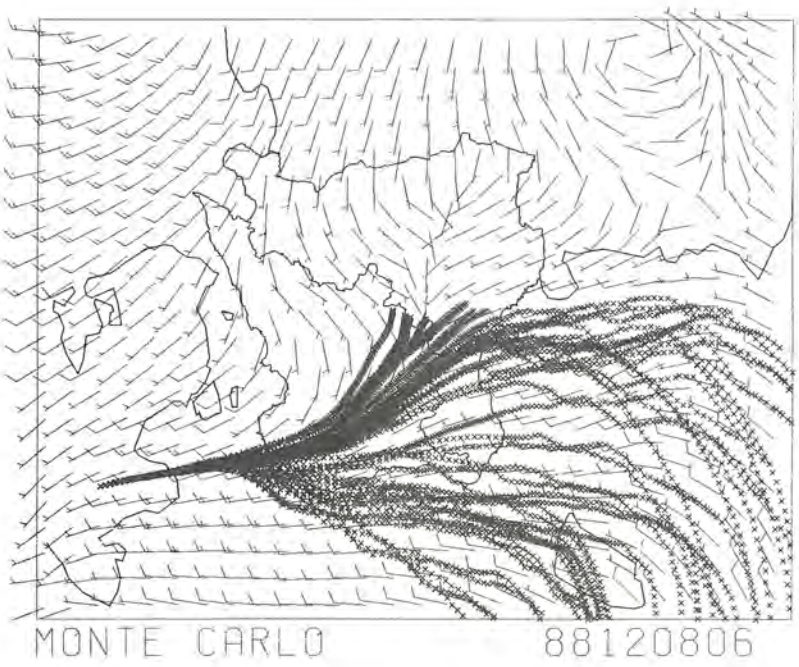

Figure 26: Dispersion experiment with a stochastic particle model. All particles at different levels are plotted together with analysed near surface wind.

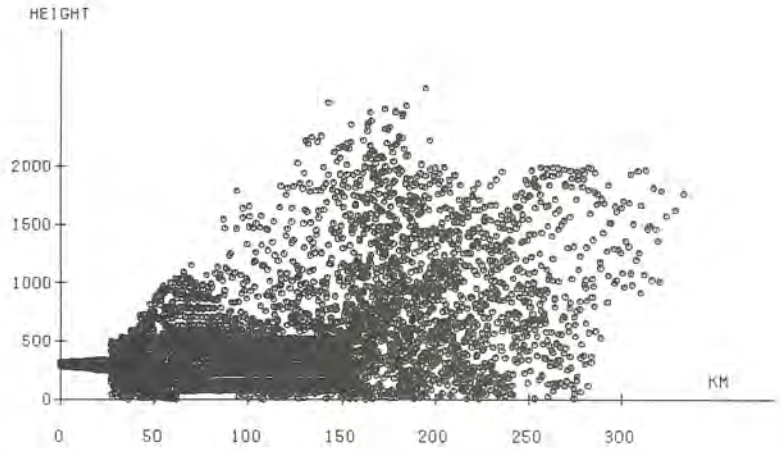

Figure 27: Dispersion experiment with a stochastic particle model. A cross-section of the plume. Each emitted particle is plotted as a function of the transported distance. Note the fumigation effect which is taking place when the plume at an early stage is crossing the coastline.

8 Concluding remarks

A system for analysis of surface parameters from a network of automatic stations to a mesoscale grid with a horizontal resolution of about 5 km was described. Display of surface fields for nowcasting purposes was initially considered the main objective of the effort. It turned out, however, that air pollution studies is another important application area.

The horizontal resolution of the analysis grid was purposly selected significantly smaller than the average station density. This was motivated since high resolution physiographic information (topography, surface roughness and land/sea thermal characteristics) is used in the generation of first guess fields as well as in the analysis structure functions.

Tuning of parameter values of the analysis structure functions was carried out by running analysis sensitivity experiments using data from a few independent observation stations for verification purposes only. From the results of these experiments the following was concluded:

- It is necessary to include the divergent part of the wind field into the analysis structure functions for a proper analysis of the 10 meter wind components.
- A reasonable first guess for the 10 meter wind analysis was obtained by computation of an Ekman wind from large-scale pressure gradients, a crude vertical stability index and a local roughness length. A dynamically interpreted first guess wind, taking also thermal effects into account, did not add any further information.
- A proper analysis of the humidity field required smaller horizontal scale lengths in the structure functions than for analysis of temperature. The analysis of the wind field indicated a similar preference for smaller scale lengths, although not as clear as for the humidity. It was difficult, if not impossible, to make any more general conclusions from the present sensitivity study. "Best" analysis were obtained in several ways, either by selecting a scale length in the structure functions or by selecting a certain signal-to-noise ratio. Taking a pragmatic approach, for the moment, reasonable analysis parameter values were derived for operational use.
- A true optimization of the values of the analysis parameters would require collection of a data base with historical time series of the observed minus first guess values. This is intended for the future.

The application of the mesoscale analysis fields in air pollution studies was illustrated by a few examples. Potential advantages in using analysis

fields in comparison with SYNOP station data were noticed. As an example, the analysis approach turned out to give wind speed values, more representative for the grid scale, for calculation of stability parameters (e.g. Monin-Obukhov length). This was particularly noted for grid squares including both land and sea areas. Another example was the application of the mesoscale analysis fields for a simple air pollution dispersion model. Output from this model indicated complicated dispersion structures, which would not have been described by a simple Gaussian approach. Therefore utilization of mesoscale analysis fields in air pollution dispersion applications certainly has a promising potential for the future.

A Boundary layer parameterizations

A.1 Model formulation 1

This formulation is mainly based on the resistance model used for rural and forest areas, while other more simple approaches are used for urban areas and water surfaces.

A.1.1 Resistance model

The classical approach to solve the energy balance equation is the Penman-Monteith formulation, or the resistance model. For the latent heat flux over a cropped surface this formulation leads to

$$\lambda E = \frac{s(Q^* - G) + (\rho C_p \delta e / r_a)}{s + \gamma(1 + (r_s/r_a))} \quad (1)$$

where λE is the latent heat flux, s is the slope of the saturation-vapor-pressure temperature curve, ρ the density of the air, C_p the specific heat at constant pressure, γ the psycrometric constant, r_a the aerodynamical resistance for sensible heat and water vapour transfer of the layer between some reference height,z, and the ground, r_s the surface resistance, and δe the saturation deficit of water vapour pressure at the reference height, Monteith [21]. The equation for the sensible heat then leads to

$$H_0 = \frac{\gamma(1 + (r_s/r_a))(Q^* - G) - (\rho C_p \delta e / r_a)}{s + \gamma(1 + (r_s/r_a))} \quad (2)$$

The surface momentum flux is defined by the friction velocity, u_*

$$\frac{\tau_0}{\rho} = u_*^2 \quad (3)$$

In order to solve the energy balance equation a parameterization has to be used for the ground flux G. The parameterization is chosen as a function of the surface sensible heat flux

$$G = \alpha_g H_0 \quad (4)$$

For open and forest areas a value of α_g of 0.3 is used.

The net radiation, Q^* is estimated following Nielsen et al [22] by empirical formulas depending on total cloud cover, N_{tot}, the amount of low,

middle and high altitude clouds, N_l, N_m and N_h, the windspeed, u, and the temperature, T, at screen height.

The surface resistance r_s is expressed according to Berkowicz and Prahm [2] and Lohammar et al [17] taken the evapotranspiration from the surface and the cannapy into account. The surface resistance due to the moisture of the surface is estimated by an empirical function of a soil moisture index, Ms, Berkowicz and Prahm [2]. The soil moisture index is determined, following Gollvik and Omstedt [15], solely by the accumulated net radiation since last rainfall, as $Ms = exp(-\int Q^* dt/C)$ where C is a coefficient assumed to be large for open areas and fairly small for forests, Gollvik and Omstedt [15]. The disadvantage of this formulation is, however, that it does not take the drying effects due to turbulent fluxes of water vapor into account.

The aerodynamical resistance r_a follows from Monin-Obukhovs similarity theory, Monin and Obukhov [20]

$$r_a = \frac{0.74}{ku_*}[ln(\frac{z_t}{z_0}) - \psi_h(\frac{z_t}{L}) + \psi_h(\frac{z_0}{L})] \tag{5}$$

where $k = 0.4$ is von Karmans constant, ψ_h is an empirical nondimentional stability function for the exchange of sensible heat, $z_t = 2$m the level where the analysed temperature is supposed to be valid, z_0 the roughness length and L Monin-Obukhovs length defined by

$$L = \frac{Tu_*^3}{gkH_0}\rho C_p \tag{6}$$

where T is the airtemperature at z_t, g is the constant of gravity and other parameters as defined above.

From similarity theory the friction velocity, u_*, can be found

$$u_* = \frac{ku}{ln(\frac{z_u}{z_0}) - \psi_m(\frac{z_m}{L}) + \psi_m(\frac{z_0}{L})} \tag{7}$$

where $z_u = 10$m is the level where the analysed windspeed, u, is valid, ψ_m is a non dimensional stability function for the exchange of momentum, and the other parameters are as defined above.

The estimates of u_*, λE and H_0 are found iteratively by help of the Monin-Obukhov length, L, until a balance of the energy balance equation is found.

A.1.2 Water surfaces

For open water surfaces a formulation according to Burridge and Gadd [5] is used. This formulation is based on a rather simple bulk approach using analysed water and air temperatures

$$\begin{aligned} H_0 &= \rho C_p C_d u(\theta_{sea} - \theta_{air}) \\ \lambda E &= \rho \lambda C_d u(q_s(T_{sea}) - q(T_{air})) \end{aligned} \tag{8}$$

where q_s is the saturation specific humidity, q is the observed specific humidity, θ the potential temperature and C_d is the drag coefficient expressed as

$$C_d = 0.001(1 - \frac{\theta_{v,sea} - \theta_v}{10}) \tag{9}$$

where θ_v is the virtual potential temperature.

For ice covered water surfaces an expression following Maykut [19] is used. Using the assumption that the flux through the ice and the latent heat flux could be omitted the following formula can be obtained

$$(1 - a)F_S + F_L^+ - \epsilon_L \sigma T_0^4 + K_s(T_a - T_0) + G_m = 0 \tag{10}$$

where a is the albedo, T_0 and T_a are the ice surface temperature and the screen level air temperature, respectively, F_S is the shortwave incoming radiation, F_L^+ is the incoming long wave radiation and the last three terms on the left hand side are the long wave outgoing radiation following Stefan-Boltzmans law, the sensible heat flux and the energy flux due to melting of ice , respectively, Maykut [19] . The exchange coefficient for sensible heat flux is defined by

$$K_s = \rho C_p C_s u \tag{11}$$

C_s is a coefficient given the value $1.2 \cdot 10^{-3}$.

The radiation fluxes, F_S and F_L^+, are calculated according to de Bruin and Wessel [4].

The energy flux balance are found iteratively with help of the ice surface temperature T_0 by the Newton-Raphson iteration method. When the surface temperature exceeds melting point, $T_0 > 0°C$ the melting term is taken

account of, and $T_0 = 0°C$, otherwise this term is omitted. Finally the sensible heat flux is detemined by

$$H_0 = -K_s(T_a - T_0). \tag{12}$$

A.1.3 Urban areas

The different energy fluxes within an urban area exhibit a very complex pattern, and are also highly site dependent. The way of treating this is to look into a volume box which extends over the buildings, covering the whole urban area. For such a box an energy budget equation could be expressed quite similar to the surface energy balance equation

$$H_0 + \lambda E = Q^* + Q_F - \Delta Q_S \tag{13}$$

where ΔQ_S is the heat flux due to storage change in the soil and the buildings, Q_F is the anthropogenic heat flux due to combustion and the other terms as defined above, Cleugh and Oke [6].

For the heat storage change (ΔQ_S) Cleugh and Oke [6] suggests a parameterization taken as a mean over several types of urban areas

$$\begin{aligned} \text{Day } (Q^* \geq 0){:}\Delta Q_S &= 0.25(Q^* - 27) \\ \text{Night } (Q^* < 0){:}\Delta Q_S &= 0.67(Q^*) \end{aligned} \tag{14}$$

The anthropogenic contribution to the sensible heat flux could with some simplifications be parameterized as a function of the air temperature

$$\begin{aligned} Q_F &= Q_{MAX} \text{ when } T < T_1 \\ Q_F &= Q_{MAX}\frac{T_0 - T}{T_0 - T_1} \text{ when } T_1 \leq T \leq T_0 \\ Q_F &= 0 \text{ when } T > T_0 \\ T_0 &= 17°C \\ T_1 &= -20°C \end{aligned} \tag{15}$$

The entity Q_{MAX} is depending on the size of the city. From measurements of anthropogenic sensible heat flux within one of the major Swedish

Parameter	Analysis needed	Surface parameters needed
Q^*	N_{tot}, N_l, N_m, N_h u, T	
Ms	Precipitation	Q^*
r_s	T, humidity	Ms, Q^*
r_a	z_0	L, u_*
H_0	T, humidity, T_{sea}	Q^*, r_s, r_a
L	T	u_*, H_0,
u_*	u, z_0	L

Table 1: Calculated parameters using the methods described in section 6.2 and their dependence on analysed meteorological data and other calculated surface parameters.

cities, Teasler [26], we have defined Q_{MAX} as a function of the area in each gridcell that is covered by the city.

$$Q_{MAX} = 125\frac{A}{A_0}\ W/m^2 \quad 25 \leq Q_{MAX} \leq 125\ W/m^2$$

where A is the area of the city and A_0 is 5 km^2.

The surface sensible heat flux and the latent heat flux are finally calculated by using the Bowen ratio, β. Several suggestions of the value of the Bowen ratio for urban areas could be found in the literature, here we have used the value 1.28 according to Cleugh and Oke [6].

A.1.4 Summary

The methods described above demand a number of analysed meteorological parameters as well as calculated surface parameters. In table 1 the total number of calculated parameters are listed and their dependence on analysed primary parameters (as temperature, windspeed, cloudiness etc.) and other parameters calculated by the methods described above.

A.2 Model formulation 2

The basic concept for this method is the modified Priestley-Taylor model. This model is used for all surface types except water surfaces.

A.2.1 Modified Priestley-Taylor model

The starting point for this model is, as well as for the resistance method , the energy balance equation and the Penman-Monteith formula. The latter is transformed in such a way that the surface and aerodynamical resistances are not explicitly described. The basic idea is to describe the surface sensible heat flux, H_0, according to the similarity theory,

$$H_0 = -\rho C_p u_* \theta_* \tag{16}$$

and then

$$\theta_* = \frac{\lambda E - (Q^* - G)}{\rho C_p u_*}. \tag{17}$$

By modelling λE, Q^*, and G a resulting value for θ_* can be found and then an estimate of the surface sensible heat flux, H_0, Van Ulden and Holtslag [28].

The method is used for land surfaces. The only separation of the different surface types is by their physical difference, as roughness length, albedo and soil moisture content. For water surfaces the method described in section A.1.2 is used.

a. Latent heat flux

The latent heat flux is described as

$$\lambda E = \alpha \left[\frac{S}{S+1}(Q^* - G) + \beta \rho \lambda \Delta q_d u_* \right] \tag{18}$$

which is a semi-empirical relation for the Penman-Monteith formula, where α and β are empirical coefficients, S is the slope of the saturation enthalpy curve $S = \partial(\lambda q_s)/\partial(C_p T)$, and Δq_d the part of the humidity deficit which is uncorrelated with the so called equilibrium evaporation $S/(S+1)(Q^* - G)$. One way to understand the meaning of Δq_d is that this

entety is vanishing when the actual evaporation is approaching the equilibrium evaporation, e.g. when the surface is wet and the air is saturated with water vapour.

The empirical coefficient α is determined as a function of the soil moisture index, Ms,

$$\alpha = 1.1 \times Ms \qquad 0 \leq Ms \leq 1. \tag{19}$$

The soil moisture is here determined by an iterative procedure that include the precipitation and the turbulent moisture heat flux as

$$Ms_{n+1} = Ms_n e^{\Delta R/R_0} - \frac{E_n \Delta t}{CN} \qquad 0 \leq Ms \leq 1. \tag{20}$$

$$n = 1, 2, \ldots, N$$

where ΔR is the accumulated precipitation during the time step $\frac{\Delta t}{N}$ and Δt is the time since last analysis hour, R_0 is a scaling coefficient describing the rate of which the surface moisture responds to precipitation, E_n is the moisture flux at iteration step n and C is a surface dependent coefficient determining the drying rate. Equation (20) is iterated from the previous to the present analysis hour corresponding to iteration number 1 and N respectively.

The iteration of equation (20) is complicated by the fact that the time evolution of E is not known at the starting point of the analysis. Moreover, E is dependent on the modification of Ms which is going to be evaluated. We have then applied an iterative process with a first guess of E_n as being constant since the last analysis hour. By equation (20) this gives a first estimate of Ms_N which can be used to evaluate a first estimate of E_N. By assuming E_n to be a linear function of E_1 and E_N a new estimate of Ms_N can be found, and so on. The values Ms_N and E_N will converge after just a few iterations.

b. Net radiation

The total net radiation is calulated from semi empirical relations for the absorption and reflection of the solar radiation, utilizing the total cloud cover and albedo. The long-wave radiation part of the total net radiation is parameterized with assumptions on black body radiation included. The formulation includes an unknown temperature at $z_r = 50$ m. This temperature is found by using surface similarity,

Surface type	R_0	C
Open area	10	1
Forrest	5	0.5
Urban area	5	0.5

Table 2: Coefficients determining the rate of which the soil moisture is responding to precipitation and evaporation, given an increase or decrease of the soil moisture.

Surface type	Albedo
Rural	0.15
Forest	0.12
Urban area	0.15
Dry snow	0.80
Wet snow	0.40

Table 3: Surface albedo

$$T_r = T_a - \frac{\theta_*}{k}[ln(\frac{z_r}{z_a}) - \psi_h(\frac{z_r}{L}) + \psi_h(\frac{z_a}{L})] \quad (21)$$

where T_a is the analysed air temperature at $z_a = 2$ m.

c. Soil heat flux

The soil heat storage change, G, is here assumined to be highly correlated with the temparature gradient of the surface layer, Van Ulden and Holtslag [28].

$$G = A_g(T_r - T_0) \quad (22)$$

where $A_g = 5\ Wm^2K^{-1}$.

According to Holtslag and Van Ulden [13] the temperature difference, $T_r - T_0$, can be parameterized as,

$$T_r - T_0 = -C_H Q^* / 4\sigma T_r \quad (23)$$

where C_H is

$$C_H = 0.31 \times \left[\frac{(1-\alpha)S + 1}{S + 1} \right] \quad (24)$$

The parameterization thus ends in a relation to the net radiation

$$G = C_G Q^* \quad (25)$$

where

$$C_G = (A_g / 4\sigma T_r) C_H . \quad (26)$$

d. Evaluation of u_* and H_0

An iterative process is used to find the balance of energy and thus the values of u_* and H_0, with the help of Monin-Obukhovs length L. In table 4 the total number of surface parameters calculated by the modified Priestley-Taylor model are listed, and their dependence on analysed routine meteorological data and other calculated surface parameters.

A.3 Mixing height

a. The neutral ABL

The depth of the neutral stationary ABL is described according to Blackadar and Tennekes [3],

$$h_n = 0.25 u_* / f \quad (27)$$

where f is the Coriolis parameter.

Parameter	Analysis needed	Surface parametars needed
H_0	p, T_a	u_*, θ_*
θ_*		E, Q^*, G, u_*
u_*	u, z_0	L
E	Ms, Q^*, G, u_* Rh	
L	T_a	u_*, H_0,
Q^*	N_{tot}, T_a	T_r, L
T_r	T_a	θ_*, L
Ms	Precipitation	E
G		Q^*, T_r

Table 4: Calculated parameters using the modified Priestley-Taylor method and their dependence on analysed meteorological data and other calculated surface parameters.

b. The stable ABL

For the stable ABL an expression following Zilitinkevich [30] is used,

$$h_s = 0.4(u_* L/f)^{1/2}. \tag{28}$$

This formulation offers some problems at high wind speeds and small values of H_0 for which L may become quite large. In order to get realistic values of h, its neutral value is used as an upper limit.

c. The unstable ABL

No adequate diagnostic equations exist for the unstable ABL. A dynamic model following Driedronks [9] is used instead. This model is a so called slab model dividing the ABL into three layers, a surface layer at the bottom and a bulk layer extending from the surface to an interfacial layer at the top of the ABL. In the bulk layer the potential temperature, Θ, is assumed to be approximately constant with height. The interfacial layer is characterized

by a positive temperature gradient, γ, and by a temperature jump, $\Delta\Theta$, at the top of the mixing layer.

The advection of temperature and turbulence is to some extent taken account for by a semi-Lagrangian advection model. The slab is followed along a trajectory ending at the gridpoint for which the depth of the ABL should be calculated. This is repeated for each gridpoint and at each timestep (i.e. each analysis hour). The trajectory is found by using wind analyses from the SMHI LAM analysis system on σ-coordinates, where one of the lowest levels is used and assumed to be representative for a mean wind of the ABL. The set of equations for the slab model may be summarized as follows:

The rate equation for h is

$$\frac{dh}{dt} = w_h + w_e \tag{29}$$

where w_h is the mean vertical wind velocity at h estimated from the equation of convergence applied to the meso-γ scale near surface wind analysis, w_e is the entrainment velocity defined as

$$w_e = -H_h/\Delta\Theta. \tag{30}$$

where H_h is the sensible heat flux at the top of the ABL as described by Driedronks [9]

$$H_h = -(0.2H_0/\rho C_p + 5.0Tu_*^3/gh) \tag{31}$$

The rate equations for Θ and $\Delta\Theta$ are

$$\frac{d\Theta}{dt} = (H_h - H_0)/h \tag{32}$$

$$\frac{d\Delta\Theta}{dt} = \gamma\frac{dh}{dt} - \frac{d\Theta}{dt} \tag{33}$$

where γ is the temperature gradient in the interfacial layer at the top of the ABL.

References

[1] Andersson, E., Gustafsson, N., Meuller, L. and Omstedt, G., 1986: Development of Meso-Scale Analysis Schemes for Nowcasting and Very Short Range Forcasting. *SMHI, Promis Report nr 1.*

[2] Berkowicz, B. and Prahm, L.P., 1982: Sensible Heat Flux Estimated from Routine Meteorological Data by the Resistance Method. *J. Appl. Meteorology*, 21, 1845-1864.

[3] Blackadar, A.K. and Tennekes, H., 1986: Asymptotic similarity in neutral barotropic planetary boundary layers. *J. Atmos. Sci.*, 25, 1015-1020.

[4] de Bruin, H.A.R and Wessel, H.R.A, 1988: A Model for the Formation and Melting of Ice on Surface Waters. *J. Appl. Met.*, 27, 164-173.

[5] Burridge, D.M. and Gadd, A.J., 1977: The Meteorological Office Operational 10-level Numerical Weather Prediction Model. *Sci. Paper No. 34*, Meteor. Office, London Road, Bracknell, Berkshire RG12 2sz, England, 1-39.

[6] Cleugh, H.A. and Oke, T.R., 1986: Suburban-rural energy balance comparisons in summer for Vancouver, B.C. *Boundary-Layer Meteor.*, 36, 351-369.

[7] Daley, R., 1985: The Analysis of Synoptic Scale Divergence by a Statistical Interpolation Procedure. *Monthly Weather Review*, 113, 1066-1079.

[8] Danard, M., 1976: A Simple Model for Mesoscale Effects of Topography on Surface Winds. *Monthly Weather Review*, 105, 572-581.

[9] Driedronks, A.G.M.,1982: Models and Observations of the Growth of the Atmospheric Boundary Layer. *Boundary-Layer Meteor.*, 3, 283-306.

[10] Hanna, S. R., Briggs, G. A. and Hosker Jr, R. P., 1982: Handbook on Atmospheric Diffusion. Published by *Technical Information Centre, U.S. Department of Energy.*

[11] Hollingsworth, A. and Lönnberg P. ,1986: The Statistical Structure of Short-range Forecast Errors as Determined from Radiosonde Data. *Tellus*, 38A, 111-161.

[12] Holtslag, A.A.M and De Bruin, H.A.R ,1988: Applied Modeling of the Nighttime Surface Energy Balance over Land. *J. Appl. Meteorology*, 27, 689-704.

[13] Holtslag, A.A.M and van Ulden, A.P.,1983: Asimple scheme for daytime estimates of the surface fluxes from routine weather data. *J. Climate Appl. Meteor.*, 22, 517-529.

[14] Gandin, L.S.,1963: Objective Analysis of Meteorological Fields. *Leningrad. Hydromet. Press.*

[15] Gollvik, S. and Omstedt, G., 1988: An Air Mass Transformation Model for Short Range Weather Forcasting, a Bulk Approach. *SMHI, Promis Report nr 8.*

[16] Gustafsson, N. and Törnevik, H., 1984: Development of an Operational System for Very Short Range Forecasting at SMHI *Proc. Nowcasting-II Symposium. Norrköping, Sweden, 3-7 Sept 1984.*

[17] Lohammar, T., Larsson, S., Linder, S. and Falk, S.O, 1980: Fast-Simulation Models of Gaseous Exchange in Scotch Pines. *Ecol. Bull.*, 32, 505-523.

[18] Lorenc, A.C., 1981: A Global Three-Dimensional Multivariate Statistical Interpolation Scheme. *Monthly Weather Review*, 109, 701-721.

[19] Maykut, G.A., 1986: The Surface Heat Balance. The geophysics of sea ice. Edit by Untersteiner, N., University of Washington.

[20] Monin, A.S. and Obukhov, A.M, 1954: Dimensionless Characteristics of Turbulence in the Atmospheric Surface Layer. *Dokl. Akad. Nauk. SSSR 93*, 223-226.

[21] Monteith, J.L.,1965: Evaporation and Environment. *Symp. Soc. Exp. Biol.*, 107, 181-191.

[22] Nielsen, L.B., Prahm, L.P., Berkowicz, R., and Condradson, K., 1981: Net Incoming Radiation Estimated from Hourly Global Radiation and/or Cloud observations. *J. Climat.*, 1, 255pp.

[23] Omstedt, G., 1984: An Operational Air Pollution Model Using Routine Meteorological Data. *SMHI-Report RMK nr 39.*

[24] Omstedt, G., 1988: An Operational Air Pollution Model. *SMHI-Report RMK nr 57.*

[25] Persson, Ch., Robertson, L., Häggkvist, K. and Meuller, L., 1990: Mesoskalig spridningsmodell - Modellanpassning till Skåneregionen. *SMHI serie Meteorologi.*

[26] Taesler, R., 1980 : A Box-model for the Urban Energy-budget. *Building Energy Management, Conventional and Solar Approaches*, Edit by Eduardo de Oliveira Fernandes et al, Pergamon Press Oxford and New York, 811-825.

[27] Undén, P., 1982 : The Swedish Limited Area Model. *SMHI Reports, Meteorology and Climatology, RMK 35.*

[28] Van Ulden, A. and Holtslag, A.A.M, 1985: Estimates of Atmosperic Boundary Layer Parameters for Diffusion Applications. *J. Clim. Appl. Meteorology*, 11, 1196-1207.

[29] Yamada, T., Kao C. J. and Bunker S., 1988: Airflow and air quality simulations over the western mountainous region with a four-dimensional data assimilation technique. *Atm. Env.* Vol.23, No 3, pp. 539-554.

[30] Zilitinkevich, S.S., 1972: On the determination of the height of the Ekman boundary layer. *Boundary-Layer Meteor.*, 3, 141-145.

SMHI Rapporter, METEOROLOGI OCH KLIMATOLOGI (RMK)

Nr 1 Thompson, T, Udin, I, and Omstedt, A
Sea surface temperatures in waters surrounding Sweden
Stockholm 1974

Nr 2 Bodin, S
Development on an unsteady atmospheric boundary layer model.
Stockholm 1974

Nr 3 Moen, L
A multi-level quasi-geostrophic model for short range weather predictions
Norrköping 1975

Nr 4 Holmström, I
Optimization of atmospheric models
Norrköping 1976

Nr 5 Collins, W G
A parameterization model for calculation of vertical fluxes of momentum due to terrain induced gravity waves
Norrköping 1976

Nr 6 Nyberg, A
On transport of sulphur over the North Atlantic
Norrköping 1976

Nr 7 Lundqvist, J-E, and Udin, I
Ice accretion on ships with special emphasis on Baltic conditions
Norrköping 1977

Nr 8 Eriksson, B
Den dagliga och årliga variationen av temperatur, fuktighet och vindhastighet vid några orter i Sverige
Norrköping 1977

Nr 9 Holmström, I, and Stokes, J
Statistical forecasting of sea level changes in the Baltic
Norrköping 1978

Nr 10 Omstedt, A, and Sahlberg, J
Some results from a joint Swedish-Finnish sea ice experiment, March, 1977
Norrköping 1978

Nr 11 Haag, T
Byggnadsindustrins väderberoende, seminarieuppsats i företagsekonomi, B-nivå
Norrköping 1978

Nr 12 Eriksson, B
Vegetationsperioden i Sverige beräknad från temperaturobservationer
Norrköping 1978

Nr 13 Bodin, S
En numerisk prognosmodell för det atmosfäriska gränsskiktet grundad på den turbulenta energiekvationen
Norrköping 1979

Nr 14 Eriksson, B
Temperaturfluktuationer under senaste 100 åren
Norrköping 1979

Nr 15 Udin, I, och Mattisson, I
Havsis- och snöinformation ur datorbearbetade satellitdata - en modellstudie
Norrköping 1979

Nr 16 Eriksson, B
Statistisk analys av nederbördsdata. Del I. Arealnederbörd
Norrköping 1979

Nr 17 Eriksson, B
Statistisk analys av nederbördsdata. Del II. Frekvensanalys av månadsnederbörd
Norrköping 1980

Nr 18 Eriksson, B
Årsmedelvärden (1931-60) av nederbörd, avdunstning och avrinning
Norrköping 1980

Nr 19 Omstedt, A
A sensitivity analysis of steady, free floating ice
Norrköping 1980

Nr 20 Persson, C och Omstedt, G
En modell för beräkning av luftföroreningars spridning och deposition på mesoskala
Norrköping 1980

Nr 21 Jansson, D
Studier av temperaturinversioner och vertikal vindskjuvning vid Sundsvall-Härnösands flygplats
Norrköping 1980

Nr 22 Sahlberg, J and Törnevik, H
A study of large scale cooling in the Bay of Bothnia
Norrköping 1980

Nr 23 Ericson, K and Hårsmar, P-O
Boundary layer measurements at Klockrike. Oct. 1977
Norrköping 1980

Nr 24 Bringfelt, B
A comparison of forest evapotranspiration determined by some independent methods
Norrköping 1980

Nr 25 Bodin, S and Fredriksson, U
Uncertainty in wind forecasting for wind power networks
Norrköping 1980

Nr 26 Eriksson, B
Graddagsstatistik för Sverige
Norrköping 1980

Nr 27 Eriksson, B
Statistisk analys av nederbördsdata. Del III. 200-åriga nederbördsserier
Norrköping 1981

Nr 28 Eriksson, B
Den "potentiella" evapotranspirationen i Sverige
Norrköping 1981

Nr 29 Pershagen, H
Maximisnödjup i Sverige (perioden 1905-70)
Norrköping 1981

Nr 30 Lönnqvist, O
Nederbördsstatistik med praktiska tillämpningar
(Precipitation statistics with practical applications)
Norrköping 1981

Nr 31 Melgarejo, J W
Similarity theory and resistance laws for the atmospheric boundary layer
Norrköping 1981

Nr 32 Liljas, E
Analys av moln och nederbörd genom automatisk klassning av AVHRR data
Norrköping 1981

Nr 33 Ericson, K
Atmospheric Boundary layer Field Experiment in Sweden 1980, GOTEX II, part I
Norrköping 1982

Nr 34 Schoeffler, P
Dissipation, dispersion and stability of numerical schemes for advection and diffusion
Norrköping 1982

Nr 35 Undén, P
The Swedish Limited Area Model (LAM). Part A. Formulation
Norrköping 1982

Nr 36 Bringfelt, B
A forest evapotranspiration model using synoptic data
Norrköping 1982

Nr 37 Omstedt, G
Spridning av luftförorening från skorsten i konvektiva gränsskikt
Norrköping 1982

Nr 38 Törnevik, H
An aerobiological model for operational forecasts of pollen concentration in th air
Norrköping 1982

Nr 39 Eriksson, B
Data rörande Sveriges temperaturklimat
Norrköping 1982

Nr 40 Omstedt, G
An operational air pollution model using routine meteorological data
Norrköping 1984

Nr 41 Persson, Christer, and Funkquist, Lennart
Local scale plume model for nitrogen oxides.
Model description.
Norrköping 1984

Nr 42 Gollvik, Stefan
Estimation of orographic precipitation by dynamical interpretation of synoptic model data.
Norrköping 1984

Nr 43 Lönnqvist, Olov
Congression - A fast regression technique with a great number of functions of all predictors.
Norrköping 1984

Nr 44 Laurin, Sten
Population exposure to So and NO_x from different sources in Stockholm.
Norrköping 1984

Nr 45 Svensson, Jan
Remote sensing of atmospheric temperature profiles by TIROS Operational Vertical Sounder.
Norrköping 1985

Nr 46 Eriksson, Bertil
Nederbörds- och humiditetsklimat i Sverige under vegetationsperioden.
Norrköping 1986

Nr 47 Taesler, Roger
Köldperioder av olika längd och förekomst.
Norrköping 1986

Nr 48 Wu Zengmao
Numerical study of lake-land breeze over Lake Vättern, Sweden.
Norrköping 1986

Nr 49 Wu Zengmao
Numerical analysis of initialization procedure in a two-dimensional lake breeze model.
Norrköping 1986

Nr 50 Persson, Christer
Local scale plume model for nitrogen oxides. Verification.
Norrköping 1986

Nr 51 Melgarejo, José W.
An analytical model of the boundary layer above sloping terrain with an application to observations in Antarctica
Norrköping 1986

Nr 52 Bringfelt, Björn
Test of a forest evapotranspiration model
Norrköping 1986

Nr 53 Josefsson, Weine
Solar ultraviolet radiation in Sweden
Norrköping 1986

Nr 54 Dahlström, Bengt
Determination of areal precipitation for the Baltic Sea
Norrköping 1986

Nr 55 Persson, Christer (SMHI), Rodhe, Henning (MISU), De Geer, Lars-Erik (FOA)
The Chernobyl accident - A meteorological analysis of how radionuclides reached Sweden
Norrköping 1986

Nr 56 Persson, Christer, Robertsson, Lennart (SMHI), Grennfelt, Peringe, Kindbom, Karin, Lövblad, Gun, och Svanberg, Per-Arne (IVL)
Luftföroreningsepisoden över södra Sverige 2 - 4 februari 1987
Norrköping 1987

Nr 57 Omstedt, Gunnar
An operational air pollution model
Norrköping 1988

Nr 58 Alexandersson, Hans, Eriksson, Bertil
Climate fluctuations in Sweden 1860 - 1987
Norrköping 1989

Nr 59 Eriksson, Bertil
Snödjupsförhållanden i Sverige - Säsongerna 1950/51 - 1979/80
Norrköping 1989

Nr 60 Omstedt, Gunnar, Szegö, Janos
Människors exponering för luftföroreningar
Norrköping 1990

Nr 61 Mueller, Lars, Robertson, Lennart, Andersson, Erik, Gustafsson, Nils
Meso-γ scale objective analysis of near surface temperature, humidity and wind, and its application in air pollution modelling
(Även serie Promis) Norrköping 1990

SMHI
Swedish meteorological and hydrological institute
S-60176 Norrköping, Sweden. Tel. +46 11 15 80 00. Telex 64400 smhi s.

ISSN 0347-2116